Volume 27
Number 30
14 August 2025
Pages 5033–5214

CrystEngComm

rsc.li/crystengcomm

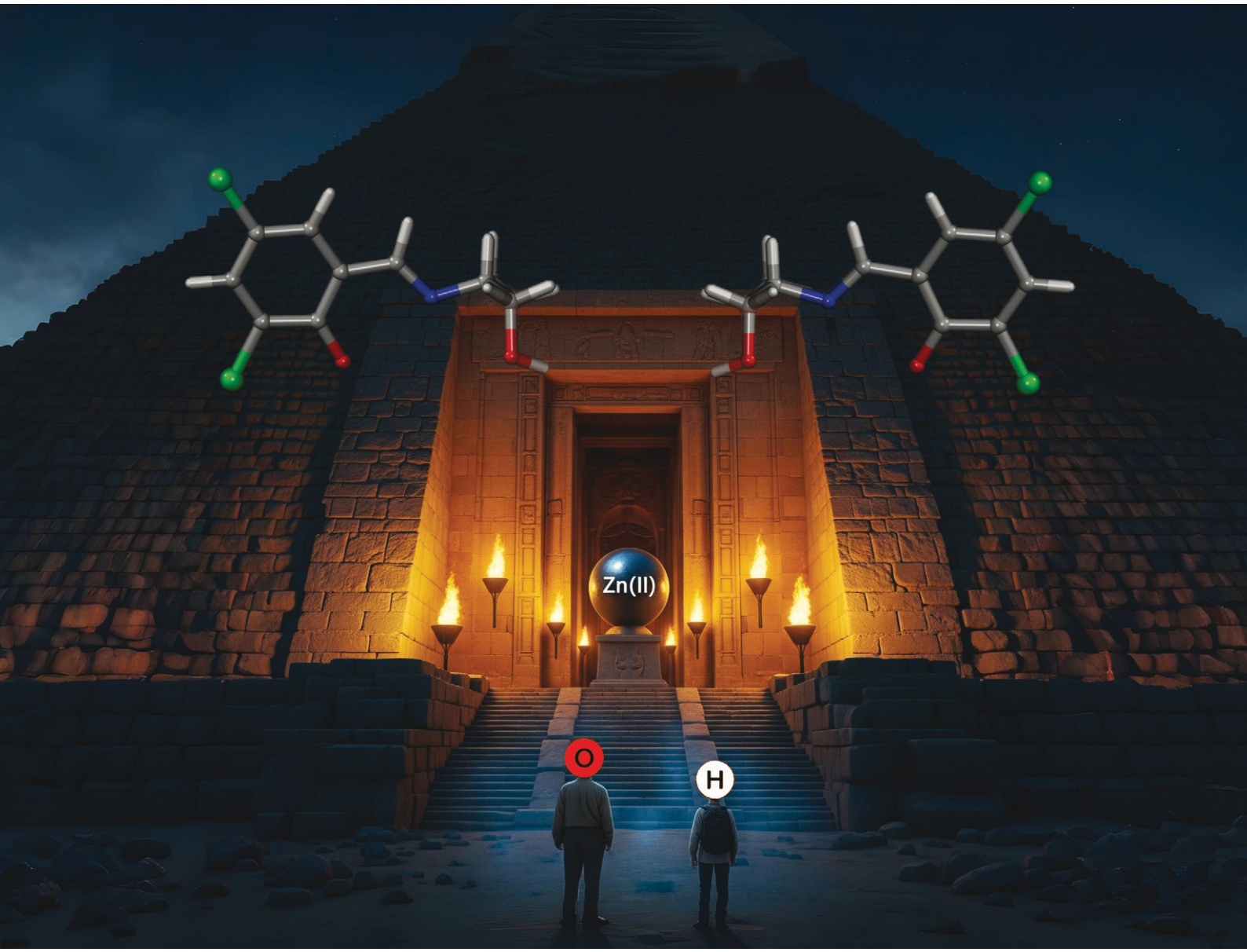

ISSN 1466-8033

ROYAL SOCIETY OF CHEMISTRY

PAPER

Shouvik Chattopadhyay *et al.*

Synthesis, structural characterization, and DFT analysis of zinc(II) Schiff base complexes featuring noncovalent spodium bonds

CrystEngComm

ROYAL SOCIETY OF CHEMISTRY

PAPER

View Article Online
View Journal | View Issue

Cite this: *CrystEngComm*, 2025, **27**, 5104

Synthesis, structural characterization, and DFT analysis of zinc(II) Schiff base complexes featuring noncovalent spodium bonds†

Md Gishan,[a] Puspendu Middya,[a] Sergi Burguera,[b] Antonio Frontera *[b] and Shouvik Chattopadhyay *[a]

Received 19th March 2025,
Accepted 6th June 2025

DOI: 10.1039/d5ce00304k

rsc.li/crystengcomm

In this study, we report the synthesis and comprehensive characterization of five novel zinc(II) complexes with Schiff base ligands: $[Zn(HL^1)_2]$ (**1**), $[Zn(HL^2)_2]\cdot DMSO\cdot 2H_2O$ (**2A**), $[Zn(HL^2)_2]\cdot DMF$ (**2B**), $[Zn_2(HL^3)_4]$ (**3**), and $[Zn_2(HL^4)_4]\cdot H_2O$ (**4**). SC-XRD confirms the structures of the complexes, revealing diverse coordination environments and noncovalent interactions, including spodium bonds. The role of hydroxyalkyl groups in stabilizing these complexes is highlighted, showing their contribution to both hydrogen and spodium bonds. Theoretical studies, including DFT geometry optimizations using periodic boundary conditions, QTAIM, and NCIPlot analyses, elucidate the nature of these weak interactions. Natural bond orbital (NBO) analysis further demonstrates charge transfer from the lone pair of oxygen atoms to the Zn(II) centers, emphasizing the polarization of the zinc orbitals. These findings advance the understanding of spodium bonding in coordination chemistry and its role in stabilizing supramolecular assemblies.

Introduction

Zinc plays a pivotal role in many biological, chemical, and material applications.[1–8] Zinc coordination complexes are integral to biological processes such as enzymatic catalysis,[9–11] structural stabilization in proteins,[12–14] and zinc-finger motifs in gene regulation.[15–17] In materials science, zinc complexes are widely explored for applications in luminescent devices,[18–20] catalysis,[21–24] and pharmaceuticals due to their unique coordination flexibility and ability to form diverse structural motifs.[25–30]

Schiff-base ligands, synthesized by the condensation of aldehydes (or ketones) and amines, have long been recognized as versatile tools in coordination chemistry.[31–37] Their ability to form stable complexes with transition metals,[38–44] combined with their tunable electronic and steric properties, has led to their use in catalysis,[45–48] magnetism,[49–53] and medicinal chemistry.[54] Schiff-base zinc complexes, in particular, offer an intriguing platform for exploring structural diversity and noncovalent interactions, which are key to understanding their functionality and potential applications.[34–36,55–60]

Noncovalent interactions are fundamental to the assembly and stabilization of crystalline materials.[37,61–64] These interactions, such as H-bonding, π stacking and σ-hole interactions (halogen bonding, chalcogen bonding, *etc.*) are pivotal in crystal engineering and supramolecular chemistry.[43,65–72] They govern the packing, stability, and properties of solid-state materials, making them essential for the design of advanced materials and molecular devices.[73] The study of these interactions provides insights into the subtle balance of forces that determine molecular recognition, self-assembly, and the formation of supramolecular architectures.[74–77]

Among noncovalent interactions, spodium bonds have recently emerged as a fascinating topic in crystal engineering.[78–84] Spodium bonds involve attractive interactions between electrophilic sites on post-transition metals group 12 and nucleophilic atoms, such as oxygen or nitrogen. These interactions, which often exhibit directional characteristics akin to hydrogen or halogen bonds, are of particular interest due to their potential role in stabilizing supramolecular assemblies and influencing molecular packing in crystalline materials.[85–87]

In this study, we report the synthesis, structure, and computational analyses of five zinc(II) complexes with Schiff base

[a] *Department of Chemistry, Jadavpur University, Kolkata 700032, India. E-mail: shouvik.chattopadhyay@jadavpuruniversity.in*
[b] *Department of Chemistry, Universitat de les Illes Balears, Carretera de Valldemossa km 7.5, 07122 Palma de Mallorca, Baleares, SPAIN. E-mail: toni.frontera@uib.es*

† Electronic supplementary information (ESI) available: Synthesis of Schiff base ligands H_2L^1–H_2L^4, ^1H and ^{13}C NMR spectroscopy, Hirshfeld surface analysis, and Fig. S1–S45. CCDC 2405586–2405590 contain the electronic supplementary crystallographic data for this paper. For ESI and crystallographic data in CIF or other electronic format see DOI: https://doi.org/10.1039/d5ce00304k

ligands. Using single-crystal X-ray diffraction, we identify spodium bonds as key interactions in two of the complexes. Theoretical studies, including periodic DFT calculations, quantum theory of atoms in molecules (QTAIM), and non-covalent interactions (NCI), were carried out to further characterize and confirm the nature of these interactions. Our findings contribute to the growing understanding of spodium bonding and its implications in crystal engineering and coordination chemistry.

Experimental

All starting materials and solvents were commercially available, of AR grade, and used as procured from Sigma-Aldrich. The details of the synthesis of ligands, H_2L^1–H_2L^4, are gathered in the ESI.†

Synthesis of the ligands

The details of the synthesis of ligands, H_2L^1–H_2L^4, are gathered in the ESI.†

Synthesis of the complexes

$[Zn(HL^1)_2]$ (1). An acetonitrile (10 mL) solution of salicylaldehyde (0.11 mL, ~1 mmol) was refluxed with 2-aminobutan-1-ol (0.1 mL, ~1 mmol) for *ca.* 2 h, leading to the formation of a yellow Schiff base ligand, H_2L^1. A few drops of acetonitrile were added to the reaction mixture to make the volume 20 mL. The acetonitrile solution (20 mL) of the ligand was added to the acetonitrile solution (5 mL) of anhydrous zinc(II) chloride (0.068 g, ~0.5 mmol) with stirring. Block-shaped yellow single crystals of complex **1** were collected by filtration after two weeks on slow evaporation.

Yield: (0.1439 g, ~64%) based on zinc(II) chloride. Anal. calc. for $C_{22}H_{28}N_2O_4Zn$ (FW: 449.85): C, 58.74; H, 6.27; N, 6.23. Found: C, 58.5; H, 6.1; N, 6.3%, FT-IR (KBr): ν_{max}/cm^{-1} 3576–3177 (O–H), 2961–2873 (C–H), 1613 (C═N), UV-vis, λ_{max}(MeOH)/nm, 361 (ε/dm^3 mol^{-1} cm^{-1} 8700). δ_H (400 MHz; $CDCl_3$; Me_4Si) 8.28 (2H, s, HC═N), 7.33 (4H, t, J = 8.1 Hz, Ph), 7.17–6.57 (4H, m, Ph), 4.94 (2H, s, –OH), 4.01–3.11 (4H, m, –CH_2–), 2.32 (2H, m, –CH–), 1.32 (4H, m, –CH_2–), 0.93 (6H, t, J = 7.4 Hz, –CH_3).

$[Zn(HL^2)_2]$·DMSO·2H_2O (2A). An acetonitrile (10 mL) solution of 3,5-dichlorosalicylaldehyde (~1 mmol, 0.191 g) was refluxed with 2-amininobutan-1-ol (0.1 mL, ~1 mmol) for *ca.* 2 h. A few drops of acetonitrile were added to the reaction mixture to make the volume 15 mL. The acetonitrile solution (15 mL) of the ligand (H_2L^2) was added to an acetonitrile solution (5 mL) of anhydrous zinc(II) chloride (0.068 g, ~0.5 mmol) with constant stirring at room temperature followed by the addition of DMSO solution (2 mL). After ten days, needle-shaped yellow crystals of complex **2A** were collected by filtration and allowed to dry in an open atmosphere.

Yield: (0.228 g, ~65%) based on zinc(II) chloride. Anal. calc. for $C_{24}H_{34}Cl_4N_2O_7SZn$ (FW: 701.78): C, 41.08; H, 4.88; N, 3.99; S, 4.57. Found: C, 41.1; H, 4.8; N, 4.2; S, 4.6%, FT-IR (KBr): ν_{max}/cm^{-1} 3535–3150 (OH), 2974–2917 (C–H), 1626 (C═N), λ_{max}(MeOH)/nm, 379 (ε/dm^3 mol^{-1} cm^{-1} 102 600), δ_H (400 MHz; $CDCl_3$; Me_4Si) 8.20 (2H, s, –HC═N–), 7.58–7.28 (2H, m, Ph), 7.21–6.97 (2H, m, Ph), 3.66 (4H, d, J = 57.0 Hz, –CH_2–), 3.34 (2H, m, CH) 2.61 (6H, s, –CH_3), 1.25 (4H, m, –CH_2–), 0.93 (6H, t, J = 7.7 Hz, –CH_3), δ_C (101 MHz; $CDCl_3$; Me_4Si) 207.04 (s, CO), 169.78 (s, –HC═N–), 134.30 (s, Ph), 133.30 (s, Ph), 127.75 (s, Ph), 118.54 (s, Ph), 77.65 (s, $CDCl_3$), 77.24 (s, $CDCl_3$), 77.04 (s, $CDCl_3$), 76.72 (s, $CDCl_3$), 76.54 (s, $CDCl_3$), 64.65 (s, –CH_2–), 40.07 (s, –CH_3), 30.94 (s, –CH_2–), 25.02 (s, –CH_2–), 10.81 (s, –CH_3).

$[Zn(HL^2)_2]$·DMF (2B). A methanol (10 mL) solution of 3,5-dichlorosalicylaldehyde (~1 mmol, 0.191 g) was refluxed with 2-amininobutan-1-ol (0.1 mL, ~1 mmol) for *ca.* 2 h. A few drops of methanol were added to the reaction mixture to make the volume 15 mL. The ligand H_2L^2 was not isolated and the methanol solution (15 mL) of the ligand was added to a methanol solution (5 mL) of zinc(II) acetate dihydrate (0.11 g, ~0.5 mmol) with constant stirring at room temperature followed by the addition of a few drops of DMF solution (2 mL). After ten days, yellow needle-shaped crystals of complex **2B** with X-ray quality clarity emerged at the beaker's bottom. These were gathered and allowed to dry naturally.

Yield: (0.2147 g, ~65%) based on zinc(II) acetate dihydrate. Anal. calc. for $C_{25}H_{31}Cl_4N_3O_5Zn$ (FW: 660.72): C, 45.45; H, 4.73; N, 6.36. Found: C, 45.4; H, 4.6; N, 6.5%, FT-IR (KBr): ν_{max}/cm^{-1} 3535–3150 (OH_2, OH), 2976–2856 (C–H), 1625 (C═N), λ_{max}(MeOH)/nm, 381 (ε/dm^3 mol^{-1} cm^{-1} 35 000).

$[Zn_2(HL^3)_4]$ (3). Ethanolamine (~1 mmol, 0.06 mL) and 5-chloro-2-hydroxybenzaldehyde (~1 mmol, 0.156 g) in 15 mL acetonitrile were refluxed for *ca.* 2 h. A few drops of acetonitrile were added to the reaction mixture to make the volume 15 mL. The ligand was not isolated and the acetonitrile solution (15 mL) of the Schiff base ligand H_2L^3 was added to an acetonitrile solution (10 mL) of zinc(II) acetate dihydrate (0.11 g, ~0.5 mmol), with constant stirring until a light yellow solution was observed. To avoid precipitation, a few drops of DMSO were added (2 mL) to the reaction mixture and then it was kept in an open atmosphere to grow single crystals. After four weeks, single yellow crystals of X-ray quality were gathered.

Yield: (0.328 g, ~71%) based on zinc(II) acetate dihydrate. Anal. calc. for $C_{36}H_{36}Cl_4N_4O_8Zn_2$ (FW: 925.27): C, 46.73; H, 3.92; N, 6.06. Found: C, 46.6; H, 3.9; N, 6.2%, FT-IR (KBr): ν_{max}/cm^{-1} 3446–3003 (OH), 2941–2834 (C–H), 1626 (C═N). λ_{max}(MeOH)/nm, 371 (ε/dm^3 mol^{-1} cm^{-1} 19 000), δ_H (400 MHz; $CDCl_3$; Me_4Si) 8.36 (1H, s, –CH═N–), 8.18 (3H, s, –CH ═N–), 7.17 (4H, m, Ph), 6.86 (8H, d, Ph), 4.11–3.51 (12H, m, –CH_2–, –OH), 2.64 (8H, m, –CH_2–).

$[Zn_2(HL^4)_4]$·H_2O (4). 3-Aminopropan-1-ol (~1 mmol, 0.08 mL) and 5-chloro-2-hydroxybenzaldehyde (~1 mmol, 0.156 g) in 20 mL methanol were refluxed for *ca.* 2 h to synthesize the Schiff base ligand, H_2L^4. The ligand was not isolated and the methanol solution (20 mL) of H_2L^4 was added to a methanol solution (5 mL) of zinc(II) acetate dihydrate (0.11 g, ~0.5 mmol) with constant stirring and the stirring was continued for *ca.* 2 h. X-ray quality yellow block single crystals were collected after three weeks.

Table 1 Crystal data and refinement details of complexes 1–4

Complex	1	2A	2B	3	4
Formula	$C_{22}H_{28}N_2O_4Zn$	$C_{24}H_{34}Cl_4N_2O_7SZn$	$C_{25}H_{31}Cl_4N_3O_5Zn$	$C_{36}H_{36}Cl_4N_4O_8Zn_2$	$C_{40}H_{44}Cl_4N_4O_9Zn_2$
Formula weight	449.85	701.78	660.72	925.27	997.37
Temperature (K)	273	130	273	273	273
Crystal system	Monoclinic	Monoclinic	Triclinic	Monoclinic	Orthorhombic
Space group	$P2_1/c$	$P2_1/c$	$P\bar{1}$	$C2/c$	$Pccn$
a (Å)	11.7255(13)	11.9713(11)	7.3148(5)	27.2641(8)	21.993(2)
b (Å)	14.4835(16)	16.7097(15)	12.0737(8)	9.4294(3)	10.4162(10)
c (Å)	13.8775(15)	15.6498(15)	17.2426(12)	17.5738(5)	18.6268(19)
α	(90)	(90)	88.103(2)	(90)	(90)
β	99.984(3)	98.033(3)	82.599(2)	123.972(1)	(90)
γ	(90)	(90)	87.794(2)	(90)	(90)
Z	4	4	2	4	4
V (Å^3)	2321.1(4)	3099.8(5)	1508.40(18)	3746.8(2)	4267.1(7)
d_{calc} (g cm^{-3})	1.287	1.504	1.455	1.640	1.553
μ (mm^{-1})	1.086	5.274	1.207	1.623	1.433
F(000)	944.0	1448.0	680.0	1888.0	2048.0
Total reflections	42 382	124 875	45 283	34 453	26 926
Unique reflections	5290	6213	5337	4213	3802
Observed data [$I > 2\sigma(I)$]	3937	6040	4856	3511	2632
No. of parameters	278	408	378	285	271
R(int)	0.0529	0.0552	0.0617	0.0593	0.0496
$^{\xi}$R1, $^{\Psi}$wR2 (all data)	0.0653, 0.1354	0.0413, 0.1087	0.0507, 0.1436	0.0438, 0.0904	0.0793, 0.1260
ξR1, ψwR2 [$I > 2\sigma(I)$]	0.0457, 0.1232	0.0412, 0.1086	0.0424, 0.1284	0.0340, 0.0852	0.0464, 0.1025
CCDC no.	2405586	2405587	2405588	2405589	2405590

(ξ)R1 = $\sum||F_o| - |F_e||/\sum|F_o|$; (ψ)wR2 = $\sum w(|F_o|^2 - |F_e|^2)^2/(\sum w|F_o|^2)^{1/2}$.

Yield: (0.403 g, ~81%) based on zinc(II) acetate dihydrate. Anal. calc. for $C_{40}H_{44}N_4O_9Cl_4Zn_2$ (FW: 997.37): C, 48.17; H, 4.45; N, 5.62. Found: C, 48.1; H, 4.4; N, 5.7%, FT-IR (KBr): ν_{max}/cm^{-1} 3449–3114 (O–H) 2940–2847 (C–H), 1626 (C=N), λ_{max}(MeOH)/nm, 369 (ε/dm^3 mol^{-1} cm^{-1} 200 000), δ_H (400 MHz; $CDCl_3$; Me_4Si) 8.20 (4H, s, –CH=N–), 7.28 (4H, s, Ph), 6.86 (8H, m, Ph), 3.83–3.48 (16H, m, –CH_2–), 1.98–1.67 (8H, m, –CH_2–), ^{13}C NMR (101 MHz, $CDCl_3$) δ 207.08 (s, CO), 171.01 (s, –CH=N), 168.23 (s, C–O), 164.16 (s, C–O), 135.07 (s, Ph), 134.03 (s, Ph), 132.08 (s, Ph), 130.34 (s, Ph), 124.43 (s, Ph), 119.20 (s, Ph), 118.60 (s, Ph), 77.35 (s, $CDCl_3$), 77.23 (s, $CDCl_3$), 77.03 (s, $CDCl_3$), 76.71 (s, $CDCl_3$), 60.08 (s, –CH_2–), 40.97 (s, –CH_2–), 33.29 (s, –CH_2–).

Physical measurements

Elemental analysis (carbon, hydrogen and nitrogen) of the complexes was performed on a PerkinElmer 240C elemental analyzer. Elemental analysis for complex **2A** was performed using a ThermoFisher Scientific Flash Smart V CHNS/O analyzer. Infrared spectra in KBr (4500–500 cm^{-1}) were recorded using a PerkinElmer RXI FT-IR spectrophotometer. Absorption spectra in methanol were recorded on Duetta-1621 fluorescence and SHIMADZU UV-1800i spectrophotometers. Emission spectra in methanol were recorded on Duetta-1621 and PerkinElmer LS 55 fluorescence spectrophotometers. ^{1}H NMR and ^{13}C NMR spectra were recorded using a BRUKER 400 MHz NMR spectrometer in $CDCl_3$ solvent. Powder X-ray diffraction patterns were recorded on well ground samples in the 2θ range of 5–50° using a BRUKER D8 Advance X-ray diffractometer with Cu Kα radiation (λ = 1.5418 Å). The details of Hirshfeld surface analysis are given in the ESI.†

X-ray crystallography

A 'Bruker D8 QUEST area detector' diffractometer equipped with graphite-monochromated Mo K_α radiation (λ = 0.71073 Å) was used for data collection of complexes **1**, **2A**, **2B**, **3** and

Table 2 Selected bond lengths (Å) of complexes 1–4

Bonds	Complex 1	Complex 2A	Complex 2B	Complex 3	Complex 4
Zn(1)–O(1)	1.909(2)	1.9999(16)	1.950(2)	2.0150(14)	2.119(3)
Zn(1)–N(1)	2.007(2)	2.0466(19)	2.011(3)	2.081(2)	2.060(3)
Zn(1)–O(1)^{ii}	—	—	—	—	2.040(3)
Zn(1)–O(3)	1.9273(18)	1.9930(16)	1.950(2)	2.3582(16)	2.027(3)
Zn(1)–O(2)	—	2.3070(18)	2.524(2)	—	—
Zn(1)–N(2)	2.008(2)	2.0411(19)	2.046(2)	—	2.045(4)
Zn(2)–O(3)	—	—	—	1.9587(16)	—
Zn(2)–N(2)	—	—	—	1.986(2)	—

Symmetry transformation = ^{ii} = 1 − x, 1 − y, 1 − z.

Table 3 Selected bond angles (°) of complexes **1**–**4**

Angles	Complex **1**	Complex **2A**	Complex **2B**	Complex **3**	Complex **4**
O(1)–Zn(1)–N(1)	96.73(8)	89.31(7)	92.85(10)	90.50(7)	85.43(13)
O(1)–Zn(1)–O(1)^{i}	—	—	—	100.18(6)	—
O(1)–Zn(1)–O(1)^{ii}	—	—	—	—	76.53(12)
O(1)–Zn(1)–N(1)^{i}	—	—	—	90.34(7)	—
N(1)–Zn(1)–N(1)^{i}	—	—	—	178.69(7)	—
N(1)–Zn(1)–N(2)	121.38(9)	147.82(8)	143.10(11)	—	124.31(14)
O(1)^{ii}–Zn(1)–O(3)	—	—	—	—	96.70(12)
O(1)^{ii}–Zn(1)–N(1)	—	—	—	—	120.77(13)
O(1)^{i}–Zn(1)–N(2)	—	—	—	—	113.00(13)
O(1)–Zn(1)–O(3)	116.37(8)	99.08(7)	108.29(9)	164.98(6)	172.74(12)
O(1)–Zn(1)–O(3)^{i}	—	—	—	94.16(6)	—
O(1)–Zn(1)–O(2)	—	164.45(7)	154.74(9)	—	—
O(1)–Zn(1)–N(2)	114.97(9)	107.03(7)	103.92(10)	—	94.01(13)
O(3)–Zn(1)–O(3)^{i}	—	—	—	71.96(6)	—
O(3)–Zn(1)–O(2)	—	87.55(6)	96.49(8)	—	—
O(3)–Zn(1)–O(4)		161.69(6)	—	—	—
O(3)–Zn(1)–N(1)	111.86(9)	114.41(7)	111.76(10)	93.89(7)	96.01(13)
O(3)–Zn(1)–N(1)^{i}	—	—	—	85.04(7)	—
O(3)–Zn(1)–N(2)	96.86(9)	90.71(7)	94.04(9)	—	91.06(13)
O(2)–Zn(1)–O(4)	—	85.95(6)	—	—	—
O(2)–Zn(1)–N(1)	—	75.14(7)	72.93(9)	—	—
O(2)–Zn(1)–N(2)	—	86.81(7)	78.51(9)	—	—
O(4)–Zn(1)–N(2)	—	71.87(7)	—	—	—
O(4)–Zn(1)–N(1)	—	80.33(7)	—	—	—
O(3)–Zn(2)–N(2)	—	—	—	95.75(8)	—
O(3)–Zn(2)–O(3)^{i}	—	—	—	90.04(7)	—
O(3)–Zn(2)–N(2)^{i}	—	—	—	131.04(9)	—
N(2)–Zn(2)–N(2)^{i}	—	—	—	115.27(8)	—

Symmetry transformation = ^{i} = 1 − *x*, *y*, 1.5 − *z*, ^{ii} = 1 − *x*, 1 − *y*, 1 − *z*.

4. The structures were solved by direct methods. Full-matrix least squares refinements on F^2 were done using the SHELXL-18/1 package.[88] Refinement of non-hydrogen atoms was done with anisotropic thermal parameters. Hydrogen atoms were constrained to ride on their parent atoms. The program SADABS was used for multi-scan empirical absorption corrections.[89] The crystallographic data and refinement details are summarised in Table 1. Selected bond lengths and angles are shown in Tables 2 and 3.

Theoretical methods

The X-ray geometries of complexes **2A** and **3** were used as starting points for optimization under periodic boundary conditions (PBC) at the RI-BP86-D3/def2-TZVP level of theory.[90–93] Geometry optimizations, energy calculations, wavefunction generation, and cube file creation were performed using the Turbomole 7.7 program.[94] The QTAIM[95] and NCIPlot[96] analyses were conducted at the same level of theory, utilizing the Multiwfn program[97] for calculations and VMD software[98] for visualization. For the NCIPlot analysis, the following settings were applied: s = 0.45, $\rho_{\text{cut-off}}$ = 0.04 a.u., and a color scale of $-0.035 \leq \text{sign}(\lambda_2)\rho \leq 0.035$ a.u. The natural bond orbital (NBO)[99] analysis was performed using the NBO 7.0 program.[100]

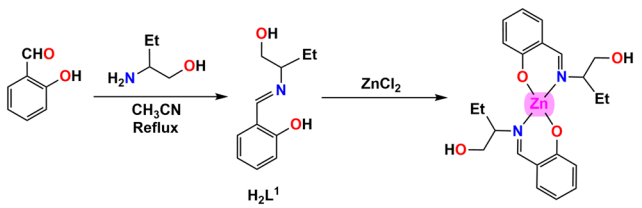

Scheme 1 Synthetic route to complex **1**.

Results and discussion

Synthesis

The N,O donor Schiff bases (HL^1–HL^4) were synthesized by refluxing the appropriate amines and salicylaldehyde

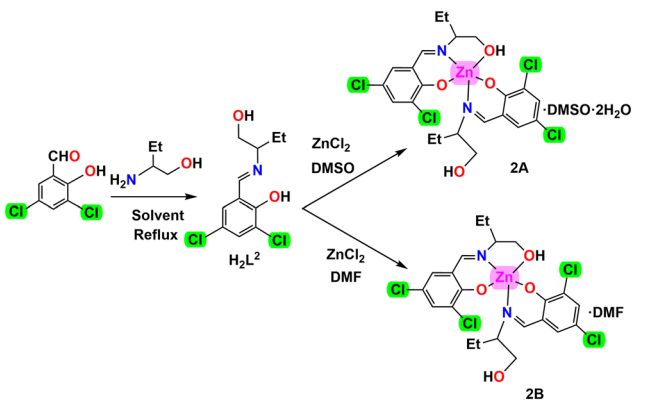

Scheme 2 Synthetic routes to complexes **2A** and **2B**.

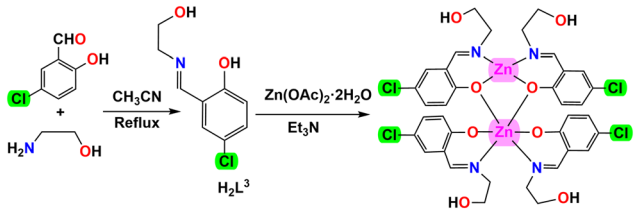

Scheme 3 Synthetic route to complex **3**.

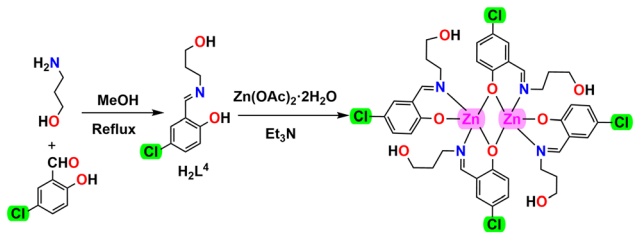

Scheme 4 Synthetic route to complex **4**.

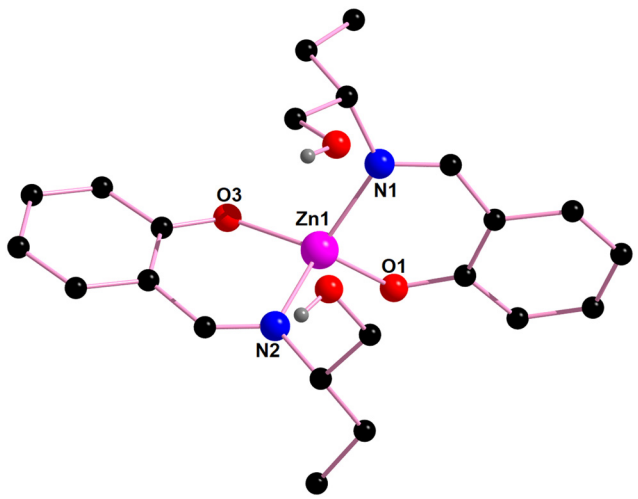

Fig. 1 The perspective view of complex **1**.

derivatives in acetonitrile/methanol following the literature methods.[59,101–109] The Schiff bases, so produced, were not isolated and not purified. These were used *in situ* for the syntheses of zinc(II) complexes $[Zn(HL^1)_2]$ (**1**), $[Zn(HL^2)_2]\cdot DMSO\cdot H_2O$ (**2A**), $[Zn(HL^2)_2]\cdot DMF$ (**2B**), $[Zn_2(HL^3)_4]$ (**3**) and $[Zn_2(HL^3)_4]\cdot H_2O$ (**4**) by adding zinc(II) chloride or zinc(II) acetate dihydrate with constant stirring for the formation of complexes **1**, **2A**, **2B**, **3** and **4** (in a 2 : 1 molar ratio). The use of drops of DMSO and DMF is essential to stabilize crystals of **2A** and **2B**, respectively. In the absence of DMSO or DMF, suitable single crystals of complexes **2A** or **2B** were not grown. This indicates the necessity of DMSO and DMF in the stabilization of the complexes. Synthetic routes to the complexes are shown in Schemes 1–4.

FT-IR spectroscopy

In the FT-IR spectrum of each complex, a distinct band for azomethine (C=N) stretching vibration appears at 1613–1626 cm^{-1}.[85,110] Bands in the region of 3000–2890 cm^{-1} may be assigned to C–H stretching vibrations.[37,111] The appearance of a broad band at around 3540–3100 cm^{-1} indicates the presence of O–H stretching vibration[112] of the hydroxyl group and lattice water molecule in each complex. The FT-IR spectra of the complexes are shown in Fig. S1–S5 (ESI†).

^1H and ^{13}C NMR spectroscopy

The detailed information of ^1H and ^{13}C NMR spectra of H_2L^1–H_2L^4 is gathered in the ESI.† The ^1H NMR spectra of H_2L^1, complex **1**, H_2L^2, complex **2A**, H_2L^3, complex **3**, H_2L^4 and complex **4** are shown in Fig. S6–S13 (ESI†), respectively. The ^{13}C NMR spectra of H_2L^1, H_2L^2, complex **2A**, H_2L^3, H_2L^4 and complex **4** are shown in Fig. S14–S19 (ESI†), respectively.

Electronic absorption spectroscopy

There is only one band in the electronic spectra of each complex in methanol (Fig. S20–S24 (ESI†)). The band at 361 nm (in **1**), 379 nm (in **2A**), 381 nm (in **2B**), 371 nm (in **3**) and

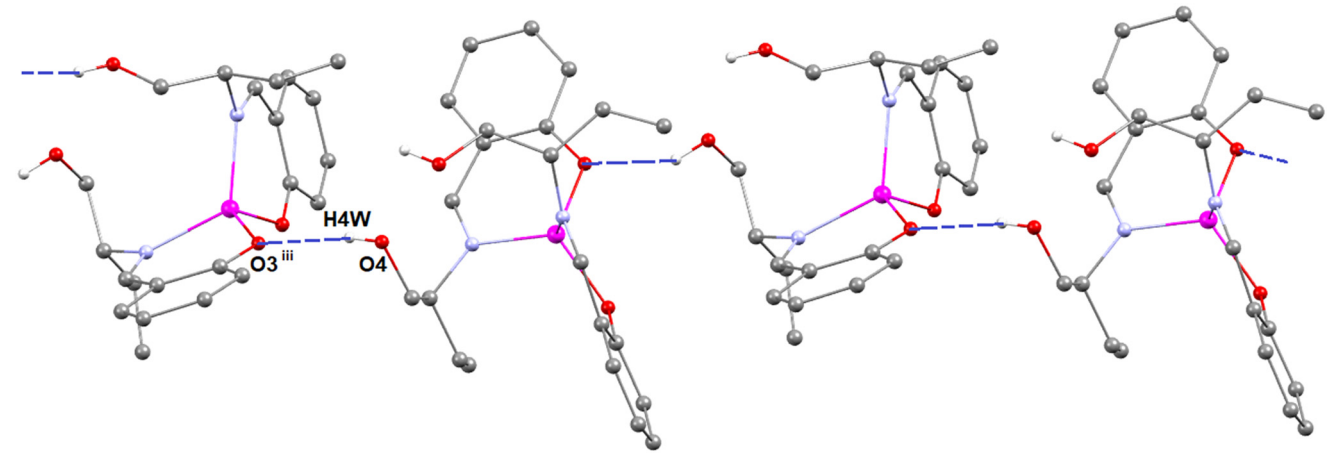

Fig. 2 Perspective view of the 1D supramolecular chain of complex **1**. Only the relevant hydrogen atoms are shown for clarity.

Table 4 O–H···O hydrogen bond distances and angles in complexes **1**, **2A**, **2B** and **3**

Complex	O–H···O	O–H (Å)	H···O (Å)	O–H···O (Å)	∠O–H···O (°)	Symmetry transformation
1	O(4)–H(4W)···O(4)^{iii}	0.820(3)	1.944	2.674(3)	147.9	^{iii} = x, 1.5 − y, ½ + z
2A	O(4)–H(4)···O(5)	0.92(4)	1.74(4)	2.624(3)	160(3)	—
	O(2)–H(2)···O(6)	0.87(5)	1.80(5)	2.663(3)	173(4)	—
	O(6)–H(6B)···O(7)	0.83(5)	1.89(5)	2.724(3)	173(5)	—
	O(7)–H(7B)···O(1)^{iv}	0.89(6)	2.04(7)	2.814(3)	145(6)	^{iv} = 1 − x, −1/2 + y, 1/2 − z
	O(7)–H(7A)···O(3)^{iv}	0.88(5)	1.97(5)	2.762(3)	149(4)	
	O(6)^{ii}–H(6A)^{ii}···O(4)	0.88(3)	2.00(3)	2.871(3)	170(3)	^{ii} = 1 − x, 1 − y, 1 − z
2B	O(4)–H(4)···O(3)^{vi}	0.820	1.978	2.776(63)	164.3	^{vi} = −1 + x, y, z
3	O(4)–H(4A)···O(3)^{vii}	1.03(5)	1.75(5)	2.751(3)	164(4)	^{vii} = x, 1 − y, 1/2 + z
	O(3)–H(3A)···O(1)	0.78(5)	1.92(5)	2.691(3)	173(4)	—

Table 5 Geometric parameters of the C–H···π interactions in complexes **1** and **2A**

Complex	C–H···π	H···π (Å)	C–H···π (Å)	∠C–H···C_g (°)	Symmetry transformation
1	C(16)–H(16)···Cg(1)^{iii}	2.748	3.980	148	^{iii} = x, 1.5 − y, 1/2 + z
2A	C(10)–H(10C)···Cg(2)^{iii}	2.908	3.658	137.07	

Cg(1)^{iii} and Cg(2)^{iii} are centroids of the aromatic rings, R(1)^{iii} {C(1)^{iii}–C(2)^{iii}–C(3)^{iii}–C(4)^{iii}–C(5)^{iii}–C(6)^{iii}} and R(2)^{iii} {C(12)^{iii}–C(13)^{iii}–C(19)^{iii}–C(20)^{iii}–C(21)^{iii}–C(22)^{iii}}.

369 nm (in **4**) is assigned to either π → π* or n → π* transitions.[59,113,114]

Structural aspects

Mononuclear zinc(II) complexes

*[Zn(HL^1)$_2$] (**1**).* Complex **1** consists of a discrete, mononuclear unit [Zn(HL^1)$_2$] (Fig. 1). The zinc(II) center is coordinated by two imine nitrogen atoms, N(1) and N(2), and two phenolate oxygen atoms, O(1) and O(3), of two tridentate N,O donor Schiff base ligands (HL^1)$^-$ producing a distorted tetrahedral structure. The τ_4 index is 0.867, which confirms that the geometry of the zinc(II) center is distorted tetrahedral {two largest ligand–metal–ligand angles are 121.38(9)° and 116.37(8)°}.[115]

Hydrogen atom H(4W) attached to oxygen atom O(4) of the Schiff base units forms a hydrogen bond with O(3)^{iii} of the symmetry related neighbouring molecule to form a 1D supramolecular chain (^{iii} = symmetry transformation = x, 1.5 − y, 1/2 + Z) (Fig. 2). The details of O–H···O hydrogen bonding interactions are summarized in Table 4.

Hydrogen atom H(16) attached to carbon atom C(16) of the Schiff base unit is involved in C–H···π interactions with the aromatic ring, R(1)^{iii} [containing carbon atoms, C(1)^{iii}–C(2)^{iii}–C(3)^{iii}–C(4)^{iii}–C(5)^{iii}–C(6)^{iii}, ^{iii} = symmetry transformation = x, 1.5 − y, ½ + z], of the neighbouring molecule to form a 1D supramolecular chain (Fig. S25, ESI†). The geometric parameters of C–H···π interactions of complex **1** are summarized in Table 5.

*[Zn(HL^2)$_2$]·DMSO·2H$_2$O (**2A**) and [Zn(HL^2)$_2$]·DMF (**2B**).* Complexes **2A** and **2B** are similar in structures, only the lattice solvent molecules are different. Both consist of mononuclear units [Zn(HL^1)$_2$] (Fig. 3 and S26, (ESI†)). Two lattice water molecules and one DMSO molecule are present in complex **2A**. On the other hand, one lattice DMF is present in complex **2B**. The zinc(II) center is coordinated by two imine nitrogen atoms [N(1), N(2)], two phenolate oxygen atoms [O(1), O(3)] of two tridentate N,O donor Schiff base ligands (HL^2)$^-$ and one hydroxyl oxygen atom O(2) of a (HL^2)$^-$ unit producing a 4 + 1 square pyramidal structure in each case (Fig. 3 and S26, (ESI†)). The square pyramidal geometry is confirmed by calculating the Addison parameters for both complexes (0.277 and 0.193 for complexes **2A** and **2B**, respectively).[116]

The saturated five-membered chelate ring [Zn(1)–N(1)–C(8)–C(11)–O(2)] represents a half-chair and an envelope conformation (Fig. S27 and S28, ESI†) with puckering parameters, q = 0.412(2) Å; ϕ = 277.5(2)° and q = 0.462(4) Å; ϕ = 283.1(4)° of complexes **2A** and **2B**, respectively.[117,118]

Six O–H···O hydrogen bonding interactions involving lattice solvent (DMSO and water) and neighbouring

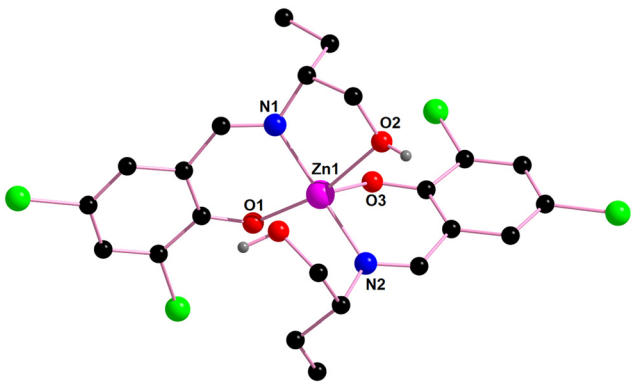

Fig. 3 Perspective view of complex **2A**. Lattice water and DMSO are not shown for clarity.

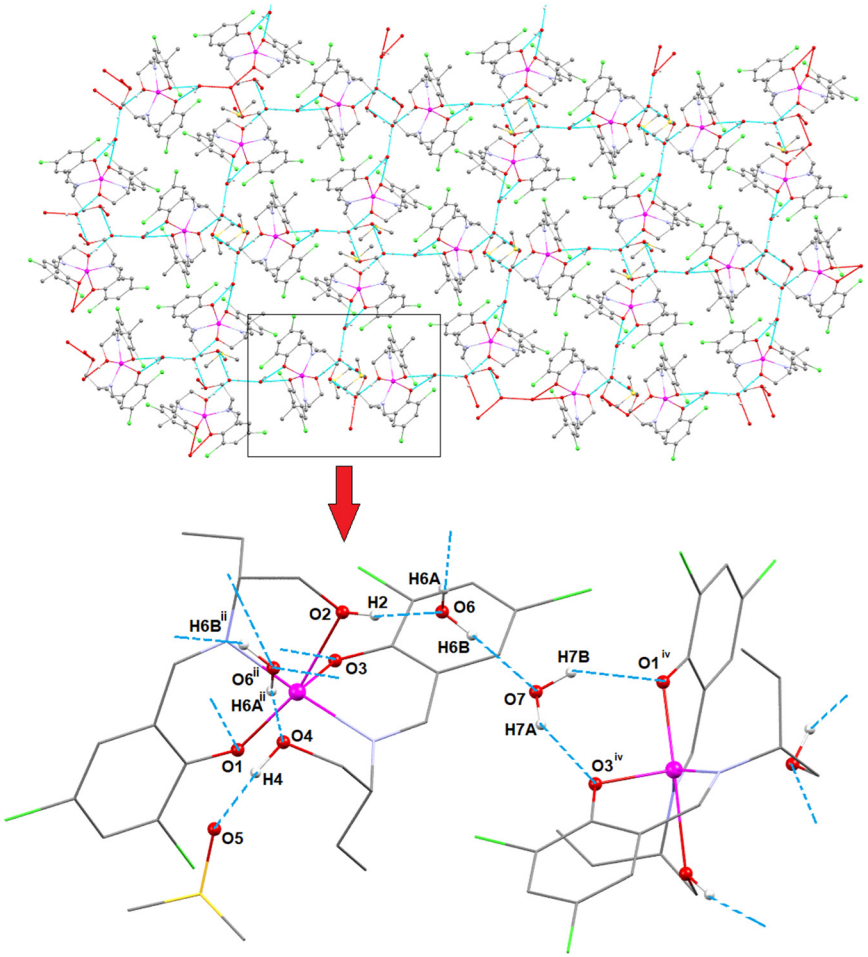

Fig. 4 2D supramolecular framework of complex **2A**, formed by O–H···O hydrogen bonding interactions.

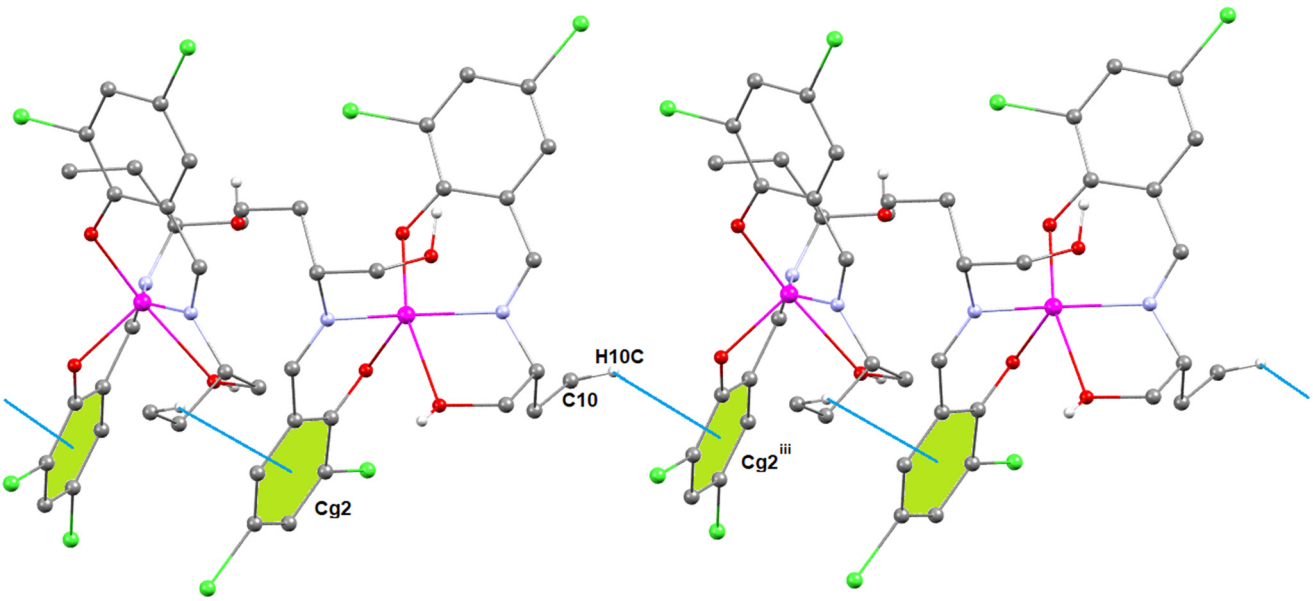

Fig. 5 C–H···π interactions of complex **2A**. Only the relevant hydrogen atoms are shown for clarity.

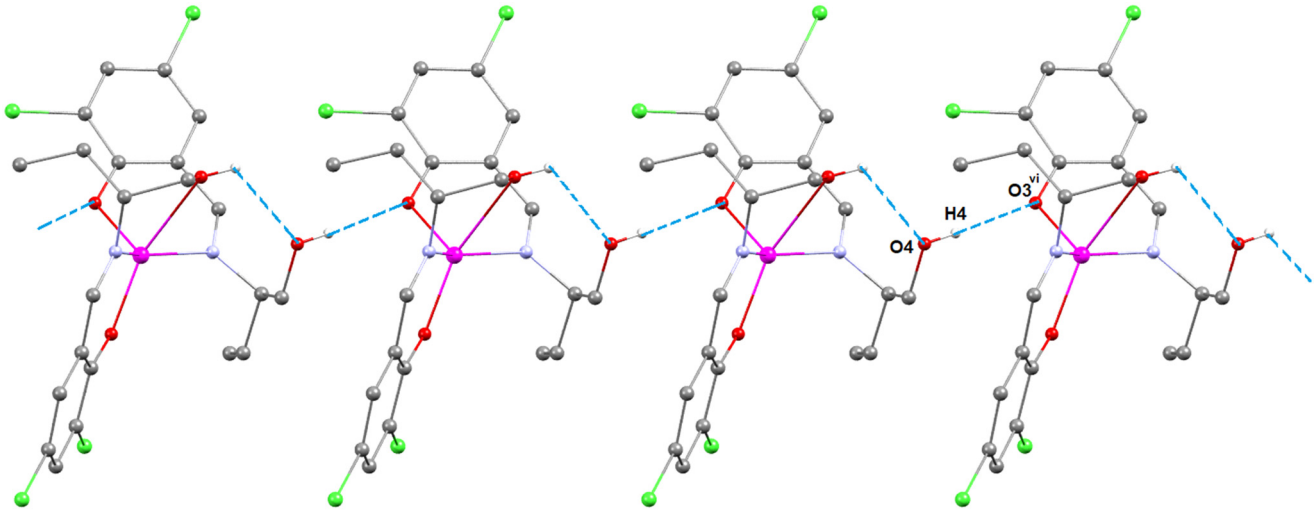

Fig. 6 Perspective view of the 1D supramolecular chain of complex **2B**, formed by O–H···O hydrogen bonding interactions.

molecules form a 2D framework of complex **2A** (Fig. 4). Hydrogen atoms H(2) and H(6B) attached to oxygen atoms O(2) and O(6) of the Schiff base unit and lattice water molecule respectively form hydrogen bonds with oxygen atoms O(6) and O(7), of the lattice water molecules. Hydrogen atoms H(7A) and H(7B) attached to oxygen atom O(7) of the lattice water molecule form hydrogen bonds with O(1)^{iv} and O(3)^{iv} of the Schiff base units of the symmetry related neighbouring molecule to form a two dimensional framework (symmetry transformation = ^{iv} = 1 − x, −1/2 + y, 1/2 + z). Hydrogen atom H(6A)^{ii} attached to O(6)^{ii} of the symmetry related lattice water molecule forms a hydrogen bond with oxygen atom O(4) of the Schiff base unit (symmetry transformation = ^{ii} = 1 − x, 1 − y, 1 − z). Hydrogen atom H(4) attached to oxygen atom O(4) of the Schiff base ligand forms a hydrogen bond with oxygen atom O(5) of the lattice DMSO molecule. The details of O–H···O hydrogen bonding interactions are gathered in Table 4.

One C–H···π interaction involving a symmetry related neighbouring aromatic ring with a hydrogen atom is observed in complex **2A**. Hydrogen atom H(10C) attached to carbon atom C(10) of the Schiff base unit is involved in C–H···π interactions with the aromatic ring, R(2)^{iii} [containing carbon atoms, C(12)^{iii}–C(13)^{iii}–C(19)^{iii}–C(20)^{iii}–C(21)^{iii}–C(22)^{iii}, ^{iii} = symmetry transformation = x, 1.5 − y, 1/2 + z], of the neighbouring molecule to form a 1D supramolecular chain (Fig. 5). The geometric parameters of C–H···π interactions of complex **2A** are gathered in Table 5.

Hydrogen atom H(4) attached to oxygen atom O(4) of the Schiff base unit forms a hydrogen bond with oxygen atom O(3)^{vi} of the symmetry related neighbouring molecule to form a 1D supramolecular chain of complex **2B** (Fig. 6). The details of O–H···O hydrogen bonding interactions are gathered in Table 4.

A π···π stacking interaction is established between the aromatic ring, R(3) {C(12)–C(13)–C(14)–C(15)–C(16)–C(17)}, forming a π···π stacking interaction with a symmetry related (^{v} = 1 − x, 1 − y, 2 − z) aromatic ring, R(3)^{v} {C(12)^{v}–C(13)^{v}–C(14)^{v}–C(15)^{v}–C(16)^{v}–C(17)^{v}}, of a neighbouring molecule to form a supramolecular dimer of complex **2B**, as shown Fig. 7.

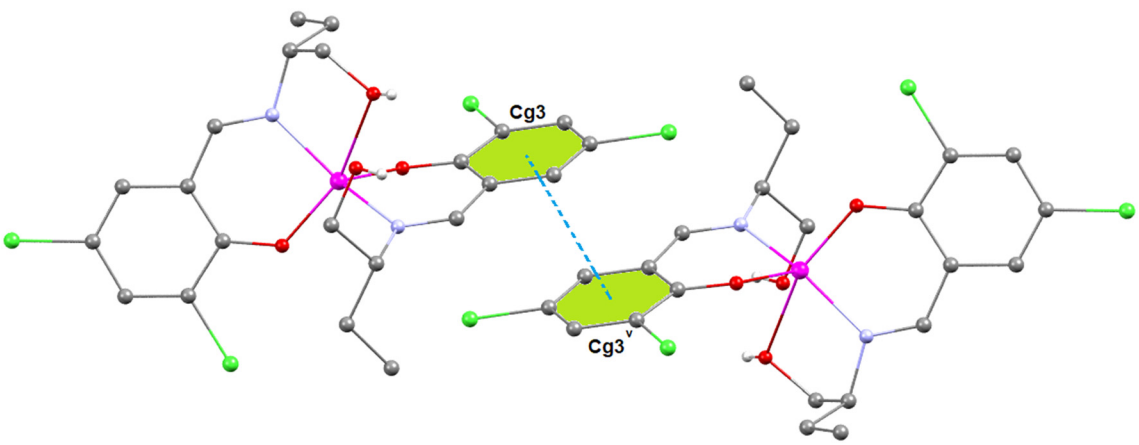

Fig. 7 Perspective view of the supramolecular dimer of complex **2B**, formed by π···π stacking interactions.

Table 6 Geometric features of the π···π stacking interactions in complexes **2B** and **4**

Complex	Cg(3)···Cg(3)^{v}/Cg(4)···Cg(4)^{viii} (Å)	Cg(3)···Perp/Cg(4)···Perp (Å)	α (°)	Slippage (Å)	Symmetry transformation
2B	3.7238(18)	3.4925(13)	0.00(15)	1.292	^{v} = 1 − x, 1 − y, 2 − z
4	3.609(3)	3.5723(18)	2.1(2)	3.380	^{viii} = 1.5 − x, 1.5 − y, z

Cg(3), Cg(3)^{v}, Cg(4) and Cg(4)^{viii} are centroids of the aromatic rings, R(3) {C(12)–C(13)–C(14)–C(15)–C(16)–C(17)}, R(3)^{v} {C(12)^{v}–C(13)^{v}–C(14)^{v}–C(15)^{v}–C(16)^{v}–C(17)^{v}}, R(4) {C(11)–C(12)–C(13)–C(14)–C(15)–C(16)} and R(4)^{viii} {C(11)–C(12)–C(13)–C(14)–C(15)–C(16)}, respectively. Cg(3)···Cg(3)^{v} = distance between ring centroids, Cg(4)···Cg(4)^{viii} = distance between ring centroids, Cg(3)···Perp = perpendicular distance of Cg(3) on ring R(3)^{v}, Cg(4)···Perp = perpendicular distance of Cg(4) on ring R(4)^{viii}, α = dihedral angle between planes R(3) and R(3)^{v} or planes R(4) and R(4)^{viii}.

The geometrical parameters of the π···π stacking interaction in complex **2B** are given in Table 6.

Dinuclear zinc(II) complexes

*[$Zn_2(HL^3)_4$] (**3**).* Based on the determination of the X-ray crystal structure, complex **3** is centrosymmetric and crystallizes in the monoclinic space group *C*2/*c*. The perspective view of complex **3** along with a selective atom-numbering scheme is shown in Fig. 8. The dinuclear complex **3** contains two different types of zinc(II) centers. Zn(1) is distorted octahedral and Zn(2) is distorted tetrahedral. Both zinc(II) centers are bridged by phenoxo oxygen atoms O(3) and O(3)^{i} of the N,O donor Schiff base ligands $(HL^3)^-$. Here, two different binding sites of the Schiff base ligands $(HL^3)^-$ have been observed, one is μ^2-η^2:η^1 to form a Zn_2O_2 core and the other binding site is η^1:η^1. The hexa-coordinated Zn(1) center bonds with four phenoxo oxygen atoms [O(1), O(1)^{i}, O(3), O(3)^{i}] and two imine nitrogen atoms [N(1) and N(1)^{i}] of four N,O donor Schiff base ligands $(HL)^-$, to form a distorted octahedral geometry. On the other hand, the tetra-coordinated Zn(2) center bonds with two phenolate oxygen atoms [O(3) and O(3)^{i}] and two imine nitrogen atoms [N(2) and N(2)^{i}] of two Schiff base ligands $(HL)^-$, to form a distorted tetrahedral geometry which is confirmed by the τ_4 index value (0.806) (where ^{i} = symmetry transformation = 1 − x, y, 1.5 − z).

Two different types of O–H···O hydrogen bonding interactions are present in complex **3**. One is an intramolecular hydrogen bond where hydrogen atom H(3A), attached to oxygen atom O(2) of the Schiff base, forms a hydrogen bond with oxygen atom O(1) of the Schiff base unit. In contrast, hydrogen atom H(4), attached to oxygen atom O(4) of the Schiff base unit, forms an intermolecular hydrogen bond with oxygen atom O(2)^{vii} of the symmetry related neighbouring molecule to form a 1D supramolecular chain (Fig. S29, ESI†) (symmetry transformation = ^{vii} = x, 1 − y, 1/2 + z). The details of O–H···O hydrogen bonding interactions are gathered in Table 4.

*[$Zn_2(HL^3)_4$]·H_2O (**4**).* Single crystal X-ray diffraction analysis reveals that complex **4** is a discrete, centrosymmetric dinuclear molecule and crystallizes in the orthorhombic space group, *Pccn*. In complex **4**, two zinc(II) centers are present {Zn(1) and Zn(1)^{ii}; ^{ii} = symmetry transformation = 1 − x, 1 − y, 1 − z}. The coordination polyhedron around the zinc(II) center is best described as a distorted trigonal bipyramidal geometry with a ZnN_2O_3 chromophore, furnished by two imine nitrogen atoms [N(1) and N(2)] and three phenolate oxygen atoms [O(1), O(1)^{ii}, O(3)] of three tridentate Schiff base ligands (^{ii} = symmetry transformation = 1 − x, 1 − y, 1 − z) (Fig. 9). The geometry around the zinc center, Zn(1), is a slightly distorted trigonal bipyramidal geometry with an Addison parameter of 0.806. The largest ligand–metal–ligand angles around the Zn(1) center are 172.7(1)° [O(1)–Zn(1)–O(3)] and 124.3(1)° [N(1)–Zn(1)–N(2)].

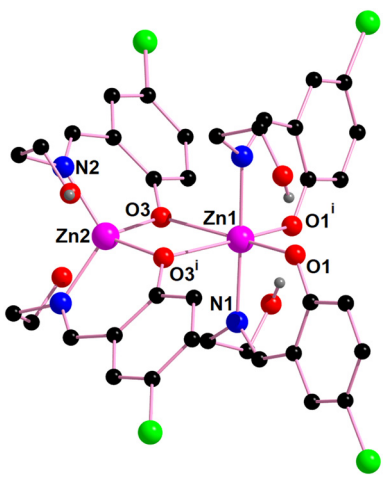

Fig. 8 Perspective view of complex **3** with selective atom numbering. Symmetry transformation ^{i} = 1 − x, y, 1.5 − z.

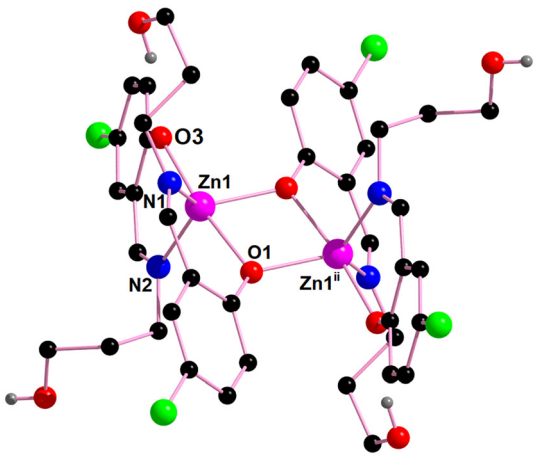

Fig. 9 Perspective view of complex **4** with selective atom numbering. Symmetry transformation ^{ii} = 1 − x, 1 − y, 1 − z.

The aromatic ring, R(4) {C(11)–C(12)–C(13)–C(14)–C(15)–C(16)}, forms a π···π stacking interaction with a symmetry related (^{viii} = 1.5 − x, 1.5 − y, z) aromatic ring, R(4)^{viii} {C(12)^{viii}–C(13)^{viii}–C(14)^{viii}–C(15)^{viii}–C(16)^{viii}–C(17)^{viii}}, of a neighbouring molecule to form a supramolecular dimer in complex **4**, as shown Fig. 10. The geometrical parameters of the π···π stacking interaction in complex **4** are given in Table 6.

Fluorescence sensing studies

Upon excitation at 361 (in **1**), 379 (in **2A**), 381 (in **2B**), 371 (in **3**) and 369 nm (in **4**) in methanol solution, the complexes show strong emission at around 468, 457, 477, 454 and 462 nm, respectively.[31] The emission of the complexes may be tentatively attributed to the intra-ligand transitions modified by metal coordination. The fluorescence spectra of the complexes are shown in Fig. S30–S34 (ESI†). The emission spectra of 10^{-3} M Schiff base ligands {H_2L^1 (excitation 397 nm, emission 446 nm) or H_2L^2 (excitation 419 nm, emission 479 nm) or H_2L^3 (excitation 397 nm, emission 454 nm) or H_2L^4 (excitation at 397 nm, emission 453 nm)} in the presence of increasing concentration of free zinc(II) at room temperature are shown in Fig. 11. The relative fluorescence intensity change profile of H_2L^1 in the presence of various cations in 10^{-2} M concentration at room temperature (excitation at 446 nm) are shown in Fig. 12. This indicates that the ligands may be used to sense zinc(II).

The relative fluorescence intensity change profiles of H_2L^2, H_2L^3, and H_2L^4 in the presence of various cations in 10^{-2} M concentration at room temperature (excitation at 479, 454 and 453 nm, respectively) are shown in Fig. S35–S37 (ESI†). From the binding interaction with zinc(II) in different Schiff base ligands H_2L^1, H_2L^2, H_2L^3 and H_2L^4, the binding constant values have been determined from the emission intensity data following the modified Benesi–Hildebrand equation:[119,120] $1/\Delta F = 1/\Delta F_{max} + (1/K[C])(1/\Delta F_{max})$. Here, $\Delta F = F_x - F_0$ and $\Delta F_{max} = F_\infty - F_0$, where F_0, F_x, and F_∞ are the fluorescence emission intensities of H_2L^1, H_2L^2, H_2L^3 and H_2L^4, considered in the absence of zinc(II), at an intermediate zinc(II) concentration and at the concentration of complete interaction, respectively, K is the binding constant and [C] is the zinc(II) ion concentration. From the plot of $(F_\infty - F_0)/(F_x - F_0)$ against $[C]^{-1}$ for H_2L^1, H_2L^2, H_2L^3 and H_2L^4 (see Fig. 13), the value of K extracted from the slopes is 0.5×10^4, 0.04×10^4, 0.05×10^4 and 0.08×10^4 M^{-1}, respectively. The above results indicate that the binding constant of H_2L^1 is higher as compared to those of H_2L^2, H_2L^2 and H_2L^4.

We have also studied the ability of the complexes to be used in the sensing of nitroaromatics. Fig. 14 illustrates that 2-nitrobenzoic acid is the best quencher towards complex **2A**. Fig. S38 (ESI†) shows the relative fluorescence intensity of various quenchers towards complex **3**. The change in relative fluorescence intensity upon the gradual increase of 10^{-2} M solution in methanol of 2-nitrobenzoic acid in 10^{-4} M solution of complex **2A** in methanol is shown in Fig. 15a.

The fluorescence responses of zinc complexes to various hazardous organic analytes, particularly nitroaromatics, underscore their potential as effective sensors in detecting and monitoring environmental pollutants. Quenching is primarily observed with nitroaromatic compounds, likely due to their highly electron-deficient nature. Fluorescence titrations of the zinc(II) complexes in MeOH were carried out by gradually increasing the concentration of various nitroaromatic compounds. The fluorescence intensity of complex **2A** kept on decreasing with increasing concentration of different nitroaromatic compounds, such as 2-nitrobenzoic acid, 2,4-dinitrophenol, and 2-hydroxy-5-nitrobenzaldehyde. Fig. 15a illustrates the fluorescence intensity quenching of complex **2A** upon the addition of 2-nitrobenzoic acid.

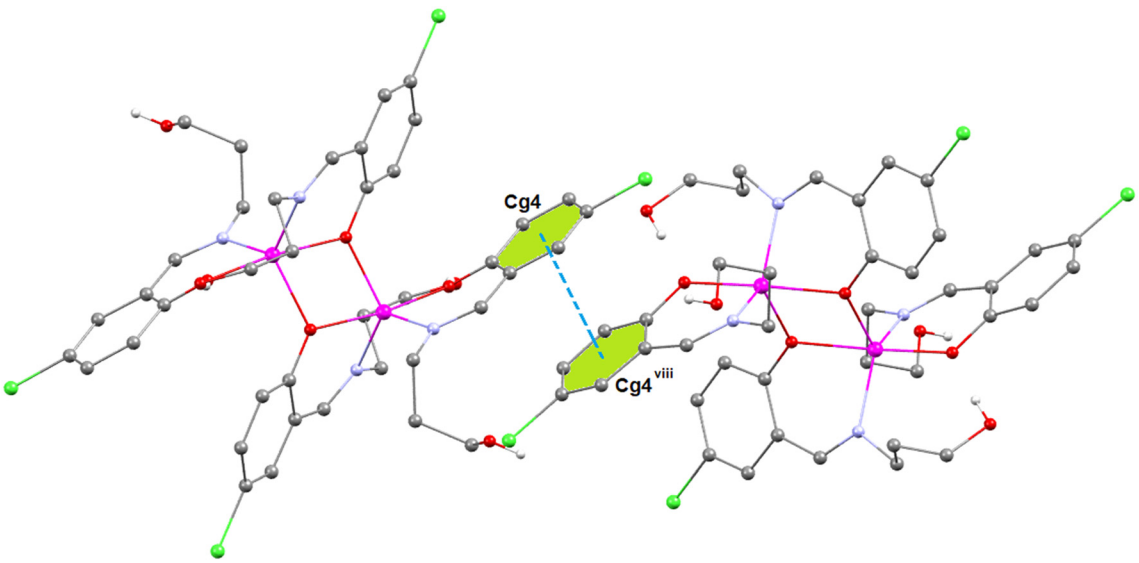

Fig. 10 Perspective view of the supramolecular dimer of complex **4**, formed by π···π stacking interactions.

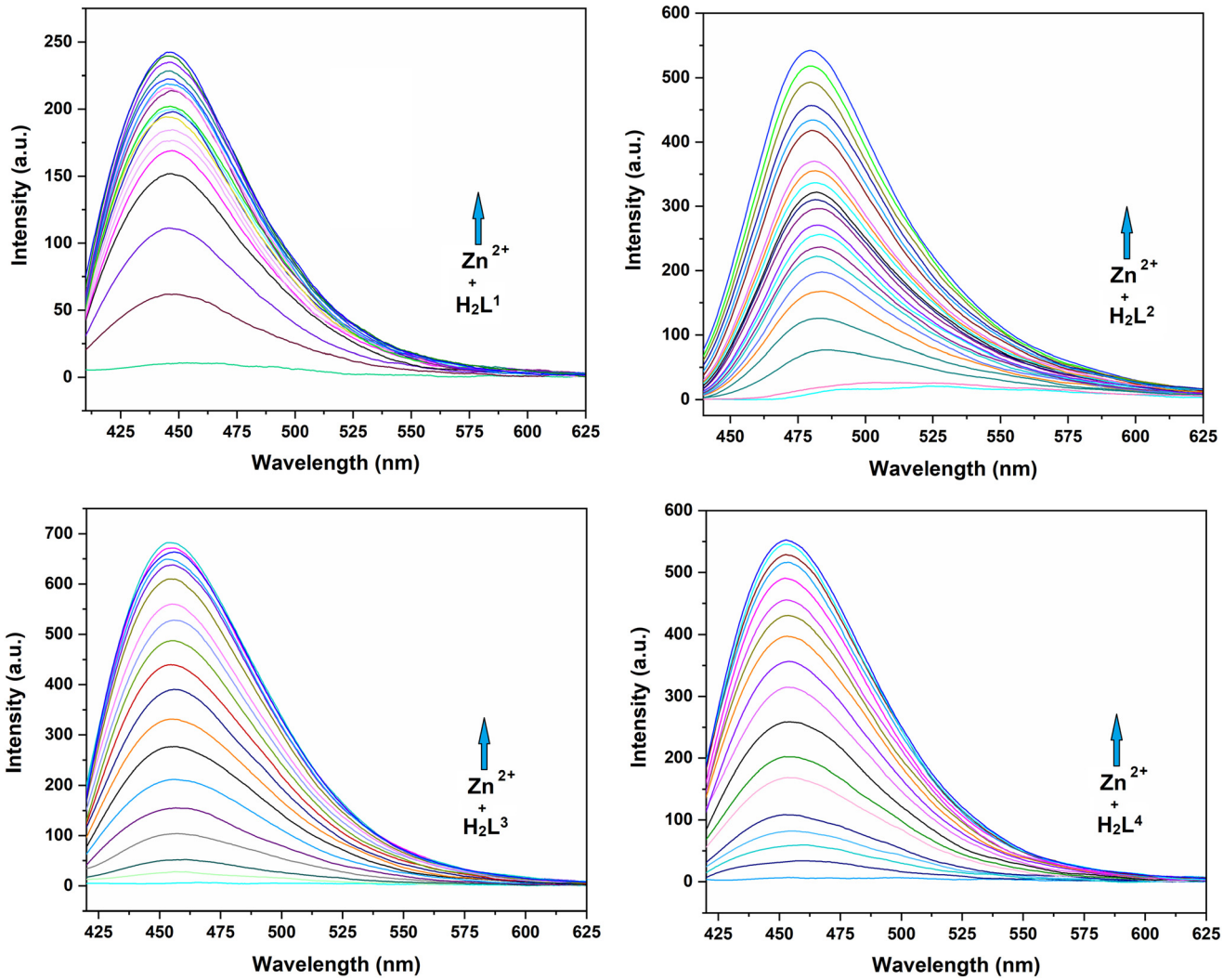

Fig. 11 Emission spectra of 10^{-3} M Schiff base ligands {H_2L^1 (excitation 397 nm, 446 nm) or H_2L^2 (excitation 419 nm, emission 479 nm) or H_2L^3 (excitation 397 nm, emission 454 nm) or H_2L^4 (excitation 397 nm, 453 nm)} in the presence of increasing concentration of free Zn^{2+} ions at room temperature.

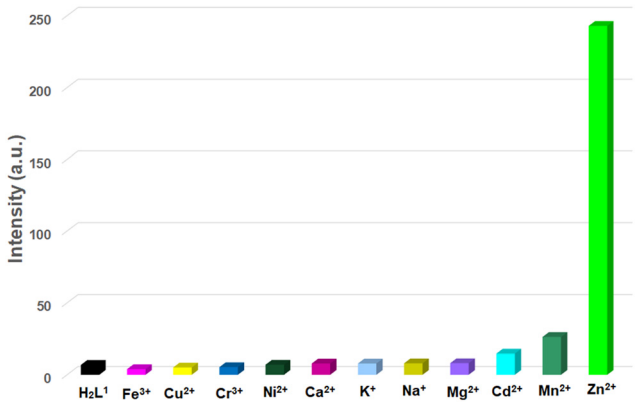

Fig. 12 Relative fluorescence intensity change profile of H_2L^1 in the presence of various cations (10^{-2} M) at room temperature (excitation at 446 nm).

The Stern–Volmer equation is employed to quantitatively assess the quenching efficiency of nitroaromatic compounds, $I_0/I = 1 + K_{SV}[Q]$, where K_{SV} = is the quencher constant (M^{-1}), [Q] is the molar concentration of the quencher, and I_0 and I are the luminescence intensities before and after quenching, respectively. When the concentration of the quencher is low, the Stern–Volmer plot of nitroaromatics is linear, in contrast, at higher concentration, it consequently deviates from linearity and turn upward (Fig. 15b), which may be due to the self-absorption.[121] The Stern–Volmer quenching constant, K_{SV}, for complex **2A** has been calculated from the slope of the linearly fitted curve (inset in Fig. 15b), equal to 0.5×10^4 M^{-1}, and the limit of detection (LOD) value is 8.81×10^{-7} (LOD = $3\sigma/k$, where σ = the standard deviation in the blank measurement,[96] and the slope (Fig. 16) from the plot (fluorescence intensity *versus* concentration of complex **2A**) gives k).

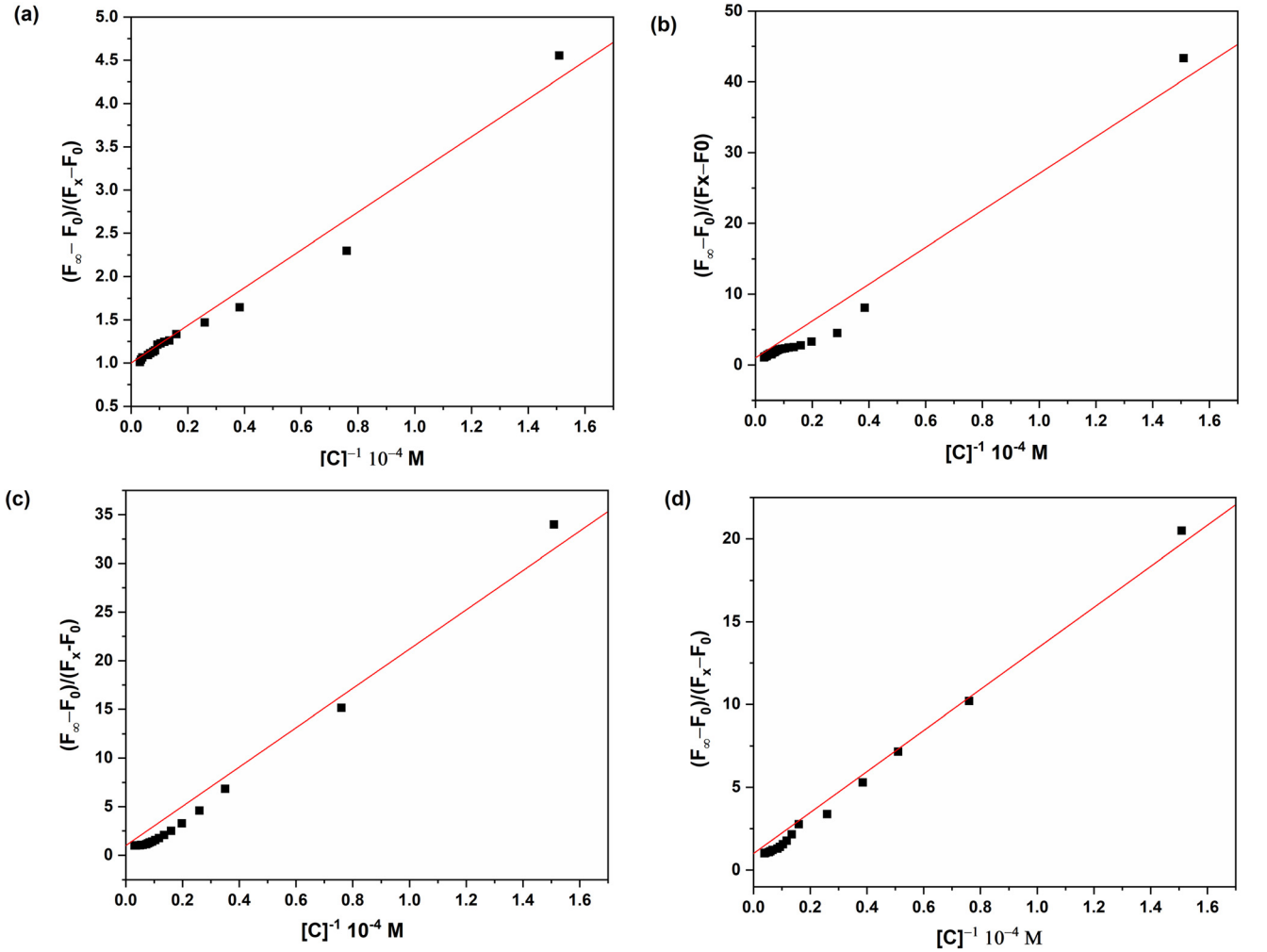

Fig. 13 Binding constants (*K*) of H_2L^1, H_2L^2, H_2L^3 and H_2L_4, determined from the slopes of the plots (a)–(d), respectively.

Nitroaromatics are electron deficient compounds. Therefore, the ability of nitroaromatics to be used as quenchers may be explained as follows. Strong π–π interactions may be established between the nitroaromatic compounds and the zinc–Schiff base complex, facilitating electron transfer from the excited state of the zinc complex to the ground state of the electron-deficient nitroaromatics.[122–127] A schematic representation of electron transfer from a zinc–Schiff base complex (say complex **2A**) to a nitroaromatic compound (*e.g.* nitrobenzene) is shown in Scheme 5a.

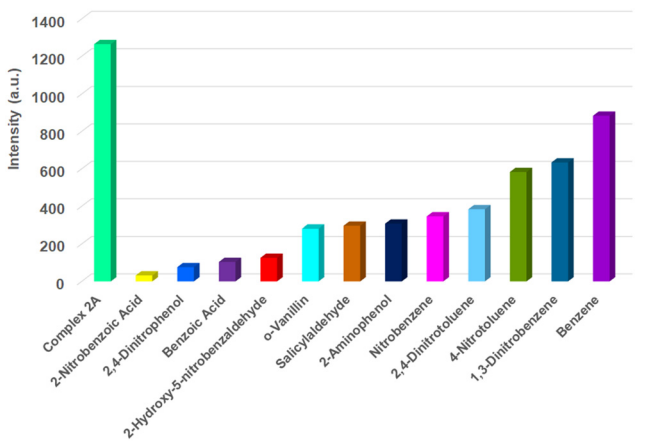

Fig. 14 Relative fluorescence intensity change profile of complex **2A** in the presence and absence of various aromatic quenchers (10^{-2} M) at room temperature (excitation at 379 nm).

If the electron deficiency of the nitroaromatic ring is further increased by the incorporation of another electron withdrawing group in its *ortho* or *para* position (with respect to the nitro group), the electron deficiency in the aromatic ring will be further reduced, and therefore, the quenching efficiency of the nitroaromatic compound will obviously be increased. This is schematically illustrated in Scheme 5b, where 2-nitrobenzoic acid containing deactivating groups, $-NO_2$ and –COOH (strong –R effect), is used as the quencher. This explains why 2-nitrobenzoic acid acts as the best quencher.

In order to give experimental evidence of this binding mechanism of nitroaromatics with the complex in solution,

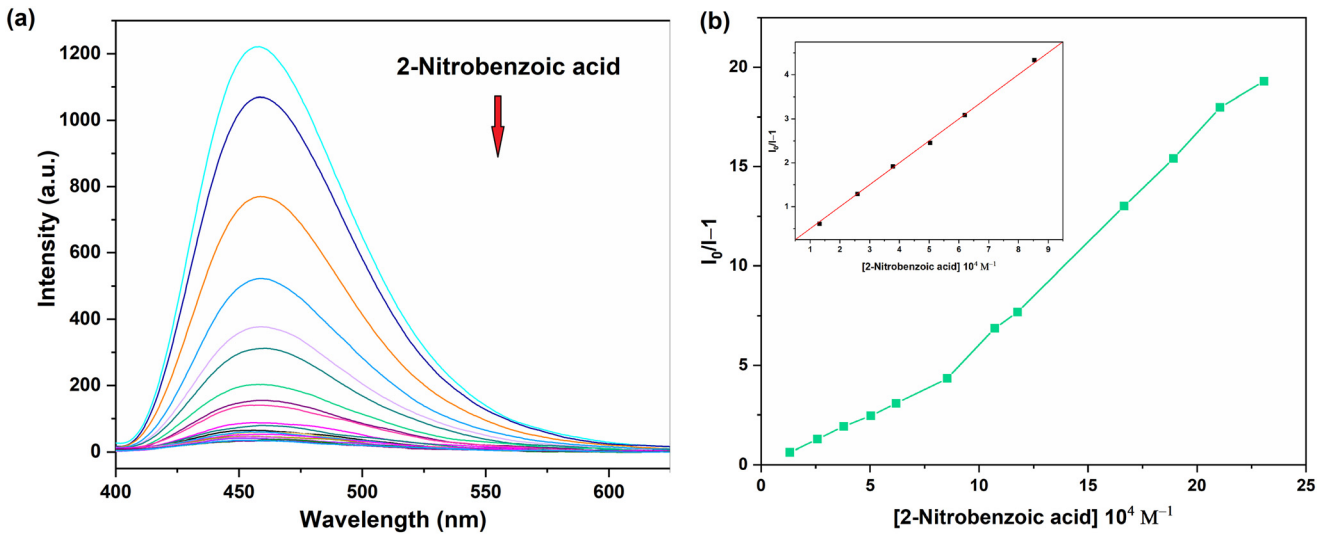

Fig. 15 (a) Fluorescence spectra of complex **2A** in MeOH (excitation wavelength of 379 nm and conc. of 10^{-4} M) with increasing concentration of 2-nitrobenzoic acid; (b) Stern–Volmer plot of complex **2A** with 2-nitrobenzoic acid in MeOH. The inset shows the linearly fitted Stern–Volmer plot with first six points.

1H NMR titration was performed with varying amounts of 2-nitrobenzoic acid (0 and 5 equiv.) in $CDCl_3$ (Fig. 17). The shifting of aromatic protons to the downfield region with increasing concentrations of nitroaromatics clearly indicates that nitroaromatics withdraw electron density from the complex and shift the protons towards the deshielded region. Except for this shifting in peak positions, everything else remains practically constant in each step of this NMR titration.

PXRD patterns

The experimental powder X ray diffraction patterns of the bulk materials are in good agreement with the simulated XRD patterns from single-crystal X-ray diffraction, indicating the consistency of the bulk sample. The simulated PXRD patterns of the complexes are computed from the single crystal structural data. Fig. S39 (ESI†) shows the experimental and simulated XRD patterns for complex **1**. Fig. S40 (ESI†) shows the experimental and simulated XRD patterns for complexes **2A** and **2B**. Fig. S41 (ESI†) shows the experimental and simulated XRD patterns for complexes **3** and **4**.

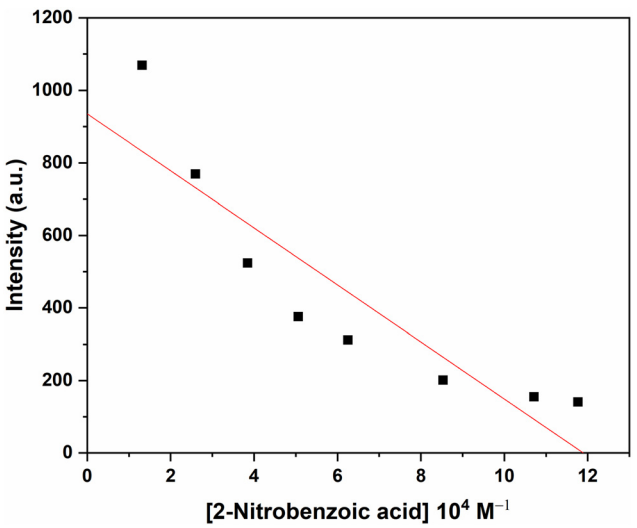

Fig. 16 Plot of limit of detection for complex **2A** towards 2-nitrobenzoic acid in MeOH solution.

DFT calculations

As described above, the zinc(II) metal centers exhibit distinct geometries and coordination indices, with the hydroxyalkyl groups of the Schiff-base ligands playing varying roles, as

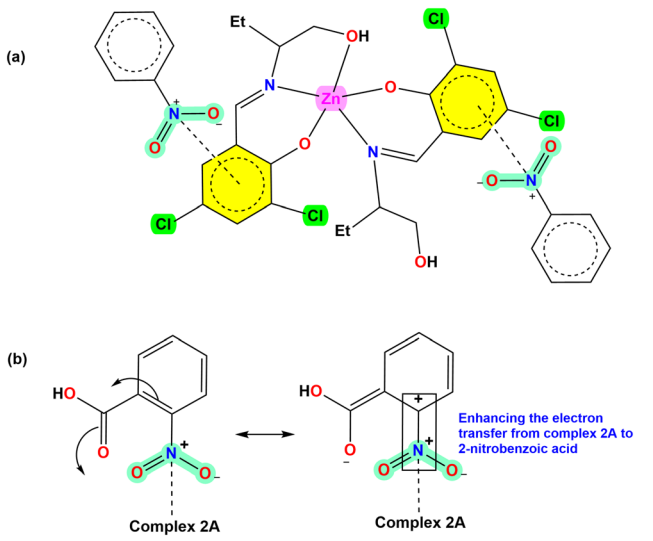

Scheme 5 (a) Schematic representation of electron transfers from complex **2A** to 2-nitrobenzoic acid; (b) schematic representation of the canonical structures of 2-nitrobenzoic acid and its impact on the quenching mechanism.

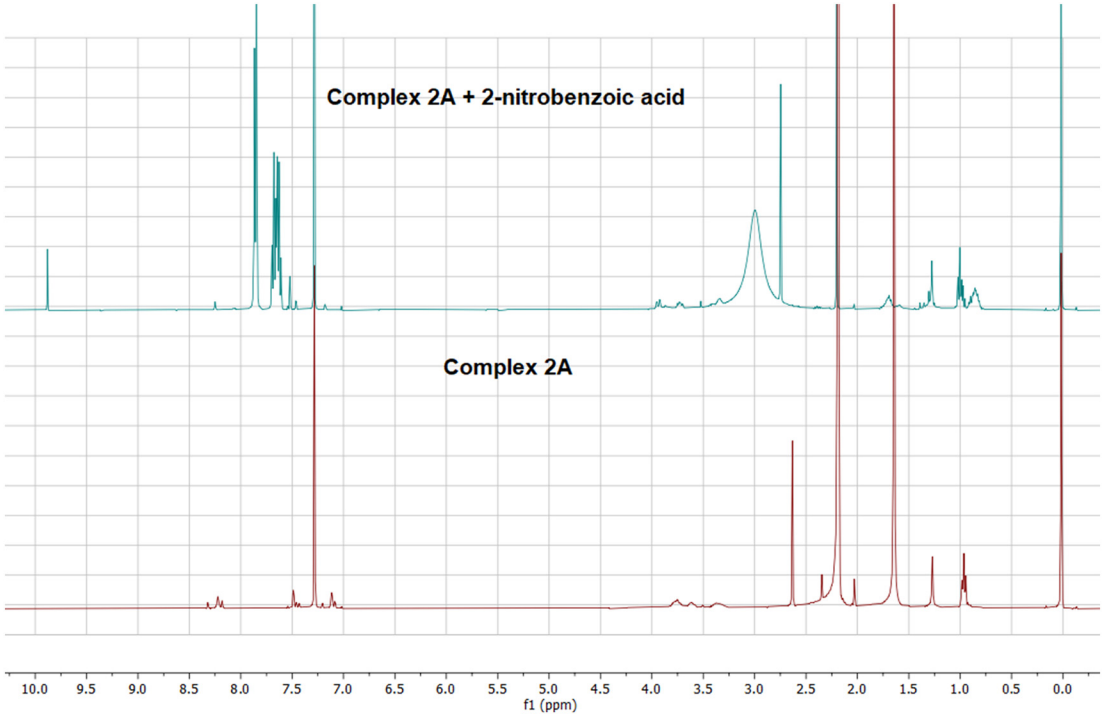

Fig. 17 ^{1}H NMR spectra of complex **2A** with 0 and 5 equivalents of 2-nitrobenzoic acid in $CDCl_3$.

detailed in Fig. 18. For instance, in the mononuclear complex **1**, the OH groups are positioned close to each other (O···O distance of 2.612 Å), indicating the formation of an OH···O hydrogen bond. A similar arrangement is observed in complex **2B**, where the uncoordinated hydroxyalkyl group interacts with the coordinated one. In contrast, in complex **2A**, which includes a crystallized DMSO molecule and two lattice water molecules, the coordinated hydroxyalkyl group forms a hydrogen bond with one water molecule, while the uncoordinated hydroxyalkyl group interacts with the DMSO molecule. This arrangement facilitates a Zn···O contact with a distance of 2.665 Å—significantly longer than the sum of covalent radii (1.88 Å) but shorter than the sum of Bondi's van der Waals radii (2.91 Å). This observation suggests the formation of a noncovalent spodium bond in this complex.

For the dinuclear complexes **3** and **4**, the positioning of the hydroxypropyl groups in complex **4** is likely governed by intramolecular hydrogen bonds. However, in complex **3**, the pseudotetrahedral Zn(II) atom establishes two symmetrically equivalent spodium bonds with the oxygen atoms of the hydroxypropyl groups, with a distance of 2.850 Å, which is close to Bondi's van der Waals radii ($\sum R_{vdw}$).

In this DFT study, we analyzed the spodium bonds in complexes **2A** and **3** using a combination of QTAIM and NCIPlot analyses. Together, these methods are effective for visualizing interactions in real space and distinguishing between attractive and repulsive interactions based on the sign of the second eigenvalue of the Hessian of the electron density (ρ). Specifically, $\lambda_2 < 0$ indicates attractive interactions, represented by blue-green reduced density gradient (RDG) isosurfaces, while $\lambda_2 > 0$ denotes repulsive interactions, shown as yellow-red RDG isosurfaces.

First, we optimized the geometries of complexes **2A** and **3** using periodic boundary conditions at the RI-BP86-D3/def2-

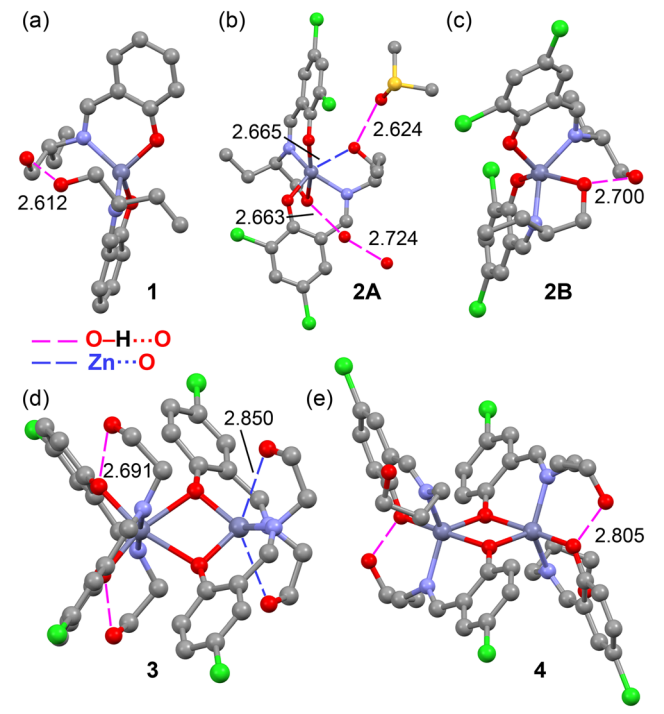

Fig. 18 Comparison of the X-ray geometries of complexes **1** (a), **2A** (b), **2B** (c), **3** (d) and **4** (e). Distances in Å. H-bonds in fuchsia and spodium bonds in dark blue dashed lines.

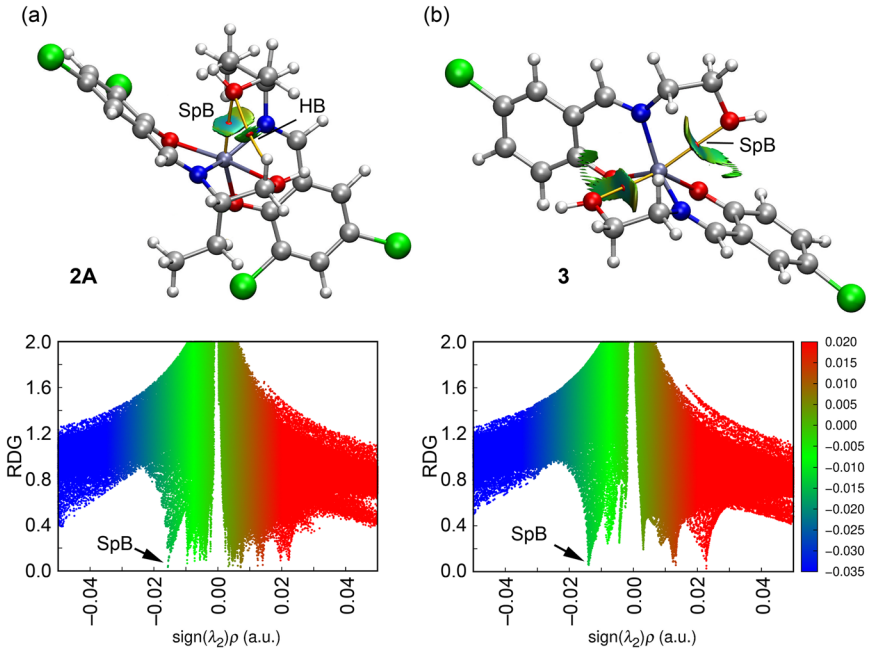

Fig. 19 Top: QTAIM distribution of BCPs and bond paths linking the hydroxyl O-atom with Zn and H-atoms in complexes **2A** (a) and **3** (b). The superimposed RDG isosurfaces are also indicated (s = 0.5, $\rho_{cut\text{-}off}$ = 0.04, color scale −0.04 a.u ≤ (sign λ_2)ρ ≤ 0.04 a.u). In complex **3**, the structure has been simplified for clarity, showing only the fragment comprising the Zn2 coordination sphere. Bottom: 2D-NCI plots for **2A** (a) and **3** (b) of reduced density gradient (RDG) *vs.* (sign λ_2)ρ with indications of the spikes corresponding to the SpBs.

TZVP level of theory. The optimized geometries closely align with the experimental structures, with Zn···O distances showing slight deviations. In **2A**, the computed Zn···O distance is 2.784 Å, which is slightly longer than the experimental value, whereas in **3**, the theoretical Zn···O distance is 2.791 Å, slightly shorter than the experimental measurement. Other geometric parameters, such as bond angles and torsions, also exhibit good agreement. For example, in **2A**, the experimental O(1)–Zn(1)–N(1) and O(1)–Zn(1)–O(3) angles are 89.31(7)° and 99.08(7)°, respectively, while the computed values are 87.8° and 99.4°. Similarly, in **3**, the experimental O(1)–Zn(1)–N(1) and O(1)–Zn(1)–O(3) angles are 90.5(7)° and 164.98(6)°, whereas the theoretical values are 90.9° and 164.0°, respectively. These results confirm the reliability of the computational method in accurately reproducing the experimental structures. Subsequently, we performed QTAIM and NCIPlot analyses, confirming in both complexes the presence of spodium bonds. The O-atom of the hydroxy group is connected to the Zn-atom through a bond critical point (red sphere in Fig. 19) and a bond path (orange line), validating the existence of these interactions.

Additionally, the spodium bonds are characterized by a blue RDG isosurface in complex **2A** and green RDG isosurfaces in complex **3**. This observation aligns with the shorter Zn···O distance in complex **2A**, indicating a stronger interaction compared to that in complex **3**. The SpBs in both complexes are also characterized by the corresponding spikes in the 2D-NCI plots of RDG *vs.* (sign λ_2)ρ, as represented in the bottom part of Fig. 19.

The QTAIM parameters at the BCP that characterize the SpBs are given in Table 7, showing that they can be classified as weak noncovalent bonds. That is, in both complexes the density values at the BCPs are small (<0.016 a.u.) and the total energy density (H) values are close to zero. Moreover, the values of the Laplacian of ρ ($\nabla^2\rho$) are small and positive. The values of λ_2 are also small and negative, indicating weak attractive interactions.

The weak nature of the SpBs has been further confirmed by calculating the energy difference between two rotamers: one corresponding to the fully optimized geometry with the SpBs intact and the other with the C–CH_2OH bond rotated to disrupt the SpBs (see Fig. 20). For complex **2A**, the energy difference is −2.4 kcal mol^{-1}, providing an estimate for the strength of a single SpB, while for complex **3**, the energy difference is −4.9 kcal mol^{-1}, corresponding to the combined contribution of two SpB contacts. These results suggest that the interactions are weak and similar in

Table 7 QTAIM in a.u. for the BCPs connecting the Zn atom to the O atom that characterize the SpBs represented in Fig. 18

Complex	BCP	$\rho(r)$	$G(r)$	$V(r)$	$H(r)$	$\nabla^2\rho(r)$	λ_2
2A	Zn1···O4	0.0157	0.0116	−0.0120	−0.0006	0.0437	−0.0124
3	Zn2···O4	0.0141	0.0110	−0.0111	−0.0001	0.0439	−0.0101

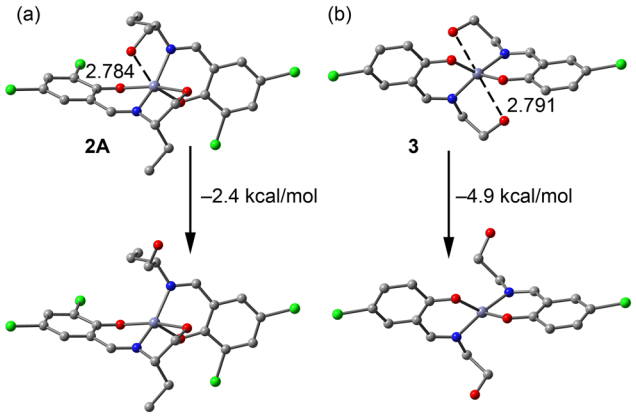

Fig. 20 Optimized structures of complexes **2A** (a) and **3** (b), indicating the energy differences between the rotamers where the Zn···O interactions are disrupted. For complex **3**, the structure has been simplified for clarity, displaying only the fragment encompassing the Zn2 coordination sphere.

strength in both systems, consistent with the comparable Zn···O distances.

However, this finding contrasts with the NCIPlot analysis, which indicated that the SpB in complex **2A** is stronger. It is important to note that evaluating SpB interactions based on energy differences between rotamers is an approximation, as other factors may influence the dihedral preference around the C–CH_2OH bond, potentially affecting the calculated energy differences.

We also analyzed the spodium bonds (SpBs) in complexes **2A** and **3** using natural bond orbital (NBO) analysis to investigate the role of charge transfer in these interactions (see Fig. 21). The analysis reveals an interesting electron donation from the lone pair orbital on the O-atom to a lone valence orbital on the Zn atom. This LP(O) → LV(Zn) charge transfer results in stabilization energies of 5.1 kcal mol^{-1} for complex **2A** (one Zn···O contact) and 6.8 kcal mol^{-1} for complex **3** (two Zn···O contacts). These findings align with the NCIPlot analysis, which showed a stronger interaction in complex **2A**, evidenced by a bluish RDG isosurface. This result also suggests that the energy of the SpBs in **3** is overestimated using the energy difference between the rotamers.

The NBO analysis further indicates that the lone valence molecular orbital receiving the electron donation corresponds to the empty 4s atomic orbital of Zn. In both complexes, this orbital is polarized toward the O-atoms, enhancing orbital overlap and facilitating the observed charge transfer. This polarization is consistent with the geometry and strength of the spodium bonds characterized in the QTAIM and NCIPlot analyses.

Conclusions

In this study, we have successfully synthesized and structurally characterized five novel zinc(II) Schiff base complexes, demonstrating diverse coordination environments and supramolecular architectures. The single-crystal X-ray diffraction analysis revealed that the complexes exhibit a range of geometries, from mononuclear tetrahedral to dinuclear distorted trigonal bipyramidal configurations. The presence of hydroxyalkyl groups and solvent molecules played a crucial role in stabilizing the crystal structures, particularly through the formation of hydrogen bonds and spodium bonds (Zn···O). The identification of spodium bonds in complexes **2A** and **3** was supported by QTAIM and NCIPlot analyses, which confirmed the noncovalent nature of these interactions. The Zn···O distances, slightly shorter than Bondi's van der Waals radii but longer than covalent radii, further emphasize the weak yet significant nature of these bonds. DFT studies using periodic boundary conditions provided excellent agreement with the experimental geometries, validating the computational approach and offering deeper insights into the electronic structure of these complexes. NBO analysis revealed that the stabilization of spodium bonds is primarily driven by LP(O) → LV(Zn) charge transfer, where the lone pair of oxygen atoms donates electron density to the empty 4s orbital of the zinc center. This charge transfer mechanism, combined with the polarization of the zinc orbitals, contributes to the overall stability of the complexes. The findings of this study advance our understanding of spodium bonding in coordination chemistry and highlight its potential role in stabilizing supramolecular assemblies. These insights could be further explored in the design of new materials with applications in

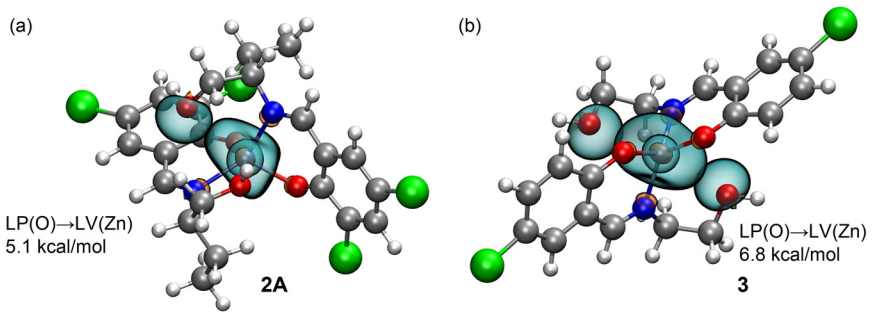

Fig. 21 Plots of the NBOs involved in the LP(O) → LV(Zn) charge transfer and the second order perturbation energies in complexes **2A** (a) and **3** (b). In complex **3**, the structure has been simplified for clarity, showing only the fragment comprising the Zn2 coordination sphere.

catalysis, molecular recognition, sensing and the development of supramolecular frameworks. Future work could focus on the systematic investigation of spodium bonds in other metal complexes and their implications in crystal engineering and materials science.

Data availability

All data underlying the results are available as part of the article and no additional source data are required.

Conflicts of interest

There are no conflicts to declare.

Acknowledgements

M. Gishan thanks UGC, India, for awarding a Junior Research Fellowship (JRF). P. Middya thanks UGC, India for awarding a Senior Research Fellowship (NFSC-SRF).

Notes and references

1 P. Roy, K. Dhara, M. Manassero, J. Ratha and P. Banerjee, Selective Fluorescence Zinc Ion Sensing and Binding Behavior of 4-Methyl-2,6-bis(((phenylmethyl)imino)methyl) phenol: BiologicalApplication, *Inorg. Chem.*, 2007, **46**, 6405–6412, DOI: **10.1021/ic700420w**.

2 X. Yan, J. J. Kim, H. S. Jeong, Y. K. Moon, Y. K. Cho, S. Ahn, S. B. Jun, H. Kim and Y. You, Low-Affinity Zinc Sensor Showing Fluorescence Responses with Minimal Artifacts, *Inorg. Chem.*, 2017, **56**, 4332–4346, DOI: **10.1021/acs.inorgchem.6b02786**.

3 T. Kokulnathan, T.-J. Wang, E. A. Kumar and Z.-U. Liu, Zinc Manganate: Synthesis, Characterization, and Electrochemical Application toward Flufenamic Acid Detection, *Inorg. Chem.*, 2021, **60**, 4723–4732, DOI: **10.1021/acs.inorgchem.0c03672**.

4 J. E. P. Brandis, S. M. Zalesak, M. A. Kane and S. L. J. Michael, Cadmium Exchange with Zinc in the Non-Classical Zinc Finger Protein Tristetraprolin, *Inorg. Chem.*, 2021, **60**, 7697–7707, DOI: **10.1021/acs.inorgchem.0c03808**.

5 O. McCubbin Stepanic, J. Ward, J. E. Penner-Hahn, A. Deb, U. Bergmann and S. DeBeer, Probing a Silent Metal: A Combined X-ray Absorption and Emission Spectroscopic Study of Biologically Relevant Zinc Complexes, *Inorg. Chem.*, 2020, **59**, 13551–13560, DOI: **10.1021/acs.inorgchem.0c01931**.

6 N. Honnaooa, A. G. Anil, S. Shekar, S. K. Behera and P. C. Ramamurthy, Design of a Highly Selective Benzimidazole-Based Derivative forOptical and Solid-State Detection of Zinc Ion, *Inorg. Chem.*, 2022, **61**, 15085–15097, DOI: **10.1021/acs.inorgchem.2c02175**.

7 T. Hirano, K. Kikuchi, Y. Urano and T. Nagano, Improvement and Biological Applications of FluorescentProbes for Zinc, ZnAFs, *J. Am. Chem. Soc.*, 2002, **124**, 6555–6562, DOI: **10.1021/ja025567p**.

8 E. Kimura and T. Koike, Recent Development of Zinc-Fluorophores, *Chem. Soc. Rev.*, 1998, **27**, 179–184, DOI: **10.1039/A827179Z**.

9 W. Maret and Y. Li, Coordination Dynamics of Zinc in Proteins, *Chem. Rev.*, 2009, **109**, 4682–4707, DOI: **10.1021/cr800556u**.

10 M. Bilal and H. M. N. Iqbal, Chemical, Physical, and Biological Coordination: An Interplay Between Materials and Enzymes as Potential Platforms for Immobilization, *Coord. Chem. Rev.*, 2019, **388**, 1–23, DOI: **10.1016/j.ccr.2019.02.024**.

11 M. J. Wiester, P. A. Ulmann and C. A. Mirkin, Enzyme Mimics Based Upon Supramolecular Coordination Chemistry, *Angew. Chem., Int. Ed.*, 2011, **50**, 114–137, DOI: **10.1002/anie.201000380**.

12 F. Namuswe and J. M. Berg, Secondary Interactions Involving Zinc-Bound Ligands: Roles in Structural Stabilization and Macromolecular Interactions, *J. Inorg. Biochem.*, 2012, **111**, 146–149, DOI: **10.1016/j.jinorgbio.2011.10.018**.

13 S. Z. Potter, H. Zhu, B. F. Shaw, J. A. Rodriguez, P. A. Doucette, S. H. Sohn, A. Durazo, K. F. Faull, E. B. Gralla, A. M. Nersissian and J. S. Valentine, Binding of a Single Zinc Ion to One Subunit of Copper–Zinc Superoxide Dismutase Apoprotein Substantially Influences the Structure and Stability of the Entire Homodimeric Protein, *J. Am. Chem. Soc.*, 2007, **129**, 4575–4583, DOI: **10.1021/ja066690**.

14 S. Gleim, A. Stojanovic, E. Arehart, D. Byington and J. Hwa, Conserved Rhodopsin Intradiscal Structural Motifs Mediate Stabilization: Effects of Zinc, *Biochemistry*, 2009, **48**, 1793–1800, DOI: **10.1021/bi800968w**.

15 A. Klug, Zinc Finger Peptides for the Regulation of Gene Expression, *J. Mol. Biol.*, 1999, **293**, 215–218, DOI: **10.1006/jmbi.1999.3007**.

16 A. Klug, The Discovery of Zinc Fingers and Their Applications in Gene Regulation and Genome Manipulation, *Annu. Rev. Biochem.*, 2010, **79**, 213–231, DOI: **10.1146/annurev-biochem-010909-095056**.

17 M. Imbeault, P.-Y. Helleboid and D. Trono, KRAB Zinc-Finger Proteins Contribute to the Evolution of Gene Regulatory Networks, *Nature*, 2017, **543**, 550–554, DOI: **10.1038/nature21683**.

18 G. Cheng, G. Kwok-Ming So, W.-P. To, Y. Chen, C.-C. Kwok, C. Ma, X. Guan, X. Chang, W.-M. Kwoke and C.-M. Che, Luminescent Zinc(II) And Copper(I) Complexes for High-Performance Solution-Processed Monochromic and White Organic Light-Emitting Devices, *Chem. Sci.*, 2015, **6**, 4623, DOI: **10.1039/C4SC03161J**.

19 R. Diana and B. Panunzi, Zinc (II) and AIEgens: The "Clip Approach" for a Novel Fluorophore Family. A Review, *Molecules*, 2021, **26**, 4176, DOI: **10.3390/molecules26144176**.

20 F. Borbone, U. Caruso, M. Causà, S. Fusco, B. Panunzi, A. Roviello, R. Shikler and A. Tuzi, Series of O,N,O-Tridentate Ligands Zinc(II) Complexes with High Solid-State Photoluminescence Quantum Yield, *Eur. J. Inorg. Chem.*, 2014, 2695–2703, DOI: **10.1002/ejic.201400095**.

21 D. Łowicki, S. Baś and J. Mlynarski, Chiral Zinc Catalysts for Asymmetric Synthesis, *Tetrahedron*, 2015, **71**, 1339–1394, DOI: **10.1016/j.tet.2014.12.022**.

22 D. J. Darensbourg and O. Karroonnium, Ring-Opening Polymerization of Lactides Catalyzed by Natural Amino-Acid Based Zinc Catalysts, *Inorg. Chem.*, 2010, **49**, 2360–2371, DOI: **10.1021/ic902271x**.

23 S. Itsuno, Y. Sakurai, K. Ito, T. Maruyama, S. Nakahama and J. M. J. Fréchet, New solid-phase catalysts for asymmetric synthesis: cross-linked polymers containing a chiral Schiff base-zinc complex, *J. Org. Chem.*, 1990, **55**, 304–310, DOI: **10.1021/jo00288a051**.

24 M. Khorshidifard, H. A. Rudbari, B. Askari, M. Sahihi, M. R. Farsani, F. Jalilian and G. Bruno, Cobalt(II), Copper(II), Zinc(II) And Palladium(II) Schiff Base Complexes: Synthesis, Characterization and Catalytic Performance in Selective Oxidation of Sulfides Using Hydrogen Peroxide Under Solvent-Free Conditions, *Polyhedron*, 2015, **95**, 1–13, DOI: **10.1016/j.poly.2015.03.041**.

25 B. Naureena, G. A. Miana, K. Shahidb, M. Asghar, S. Tanveer and A. Sarwar, Iron (III) and Zinc (II) Monodentate Schiff Base Metal Complexes: Synthesis, Characterisation and Biological Activities, *J. Mol. Struct.*, 2021, **1231**, 129946, DOI: **10.1016/j.molstruc.2021.129946**.

26 H. Kargar, M. Fallah-Mehrjardi, R. Behjatmanesh-Ardakani, H. A. Rudbari, A. A. Ardakani, S. Sedighi-Khavidak, K. S. Munawarf, M. Ashfaq and M. N. Tahir, Binuclear Zn(II) Schiff Base Complexes: Synthesis, Spectral Characterization, Theoretical Studies and Antimicrobial Investigations, *Inorg. Chim. Acta*, 2022, **530**, 120677, DOI: **10.1016/j.ica.2021.120677**.

27 A. M. Abu-Dief, R. M. El-khatibb, F. S. Aljohani, S. O. Alzahrani, A. Mahrana, M. E. Khalifac and N. M. El-Metwaly, Synthesis and Intensive Characterization for Novel Zn(II), Pd(II), Cr(III) And VO(II)-Schiff Base Complexes; DNA-Interaction, DFT, Drug-Likeness and Molecular Docking Studies, *J. Mol. Struct.*, 2021, **1242**, 130693, DOI: **10.1016/j.molstruc.2021.130693**.

28 M. Murugaiyan, S. P. Mani and M. A. Sithique, Zinc(II) Centered Biologically Active Novel N,N,O Donor Tridentate Water-Soluble Hydrazide-Based O-Carboxymethyl Chitosan Schiff Base Metal Complexes: Synthesis And Characterization, *New J. Chem.*, 2019, **43**, 9540–9554, DOI: **10.1039/C9NJ00670B**.

29 F. Ramilo-Gomes, Y. Addis, I. Tekamo, I. Cavaco, D. L. Campos, I. F. R. Pavan, C. S. B. Gomes, V. Brito, A. O. Santos, F. Domingues, Â. Luís, M. M. Marques, J. C. Pessoa, S. Ferreira, S. Silvestre and Isabel Correia, Antimicrobial and Antitumor Activity of S-Methyl Dithiocarbazate Schiff Base Zinc(II) Complexes, *J. Inorg. Biochem.*, 2021, **216**, 111331, DOI: **10.1016/j.jinorgbio.2020.111331**.

30 S. Chakraborty, C. R. Bhattacharjee, P. Mondal, S. Krishna Prasad and D. S. Shankar Rao, Synthesis and Aggregation Behaviour of Luminescent Mesomorphic Zinc(II) Complexes with 'Salen' Type Asymmetric Schiff Base Ligands, *Dalton Trans.*, 2015, **44**, 7477–7488, DOI: **10.1039/C4DT03989K**.

31 P. Middya, R. M. Gomila, A. Frontera and S. Chattopadhyay, Host–Guest Interactions in the Solid State Structure of a Zinc(II) Compound with a Protonated Diamine and DFT Study, *Inorg. Chem. Commun.*, 2023, **157**, 111436, DOI: **10.1016/j.inoche.2023.111436**.

32 P. Middya, D. Medda and S. Chattopadhyay, An Overview of the Synthesis, Structures and Applications of Di and Polynuclear Zinc-Salen Complexes with Zn_2O_2 Cores, *Inorg. Chim. Acta*, 2023, **554**, 121540, DOI: **10.1016/j.ica.2023.121540**.

33 T. Basak, S. Roy, S. Banerjee and S. Chattopadhyay, Synthesis and Characterization of Two Polynuclear Zinc(II) Complexes and Their Applications in Nitroaromatics Sensing: An Experimental and Theoretical Study, *Inorg. Chim. Acta*, 2022, **543**, 121186, DOI: **10.1016/j.ica.2022.121186**.

34 T. Basak, S. Roy, S. Banerjee, R. M. Gomila, A. Frontera and S. Chattopadhyay, Synthesis, Characterization and Selfassembly of Dinuclear Zinc Schiff Base Complexes: A Combined Experimental and Theoretical Study, *Polyhedron*, 2022, **225**, 116044, DOI: **10.1016/j.poly.2022.116044**.

35 T. Basak, A. Frontera and S. Chattopadhyay, Synthesis and Characterization of a Mononuclear Zinc(II) Schiff Base Complex: On The Importance of C–H···Π Interactions, *RSC Adv.*, 2021, **11**, 30148–30155, DOI: **10.1039/D1RA03943A**.

36 M. Karmakar, A. Frontera and S. Chattopadhyay, Insight into the Formation of H-Bonds Propagating the Monomeric Zinc Complexes of a Tridentate Reduced Schiff Base to form an Infinite Chain, *CrystEngComm*, 2021, **23**, 1918–1928, DOI: **10.1039/D0CE01840F**.

37 I. Mondal, T. Basak, S. Banerjee and S. Chattopadhyay, A Theoretical Insight On the Rigid Hydrogen-Bonded Network in The Solid State Structure of Two Zinc(Ii) Complexes and Their Strong Fluorescence Behaviors, *CrystEngComm*, 2020, **22**, 3005–3019, DOI: **10.1039/D0CE00125B**.

38 S. Bhunia, S. Jana, R. M. Gomila, M. G. B. Drew, A. Frontera and S. Chattopadhyay, An Insight into The Non-Covalent Cl···Cl Interaction in The Solid State Structure of Carboxylate Bridged Trinuclear Mixed Valence Cobalt(III/II/III) Complexes with Tetradentate N2O2 Donor Reduced Schiff Base Ligands, *Polyhedron*, 2024, **255**, 116964, DOI: **10.1016/j.poly.2024.116964**.

39 T. Dutta, S. Mirdya, P. Giri and S. Chattopadhyay, Synthesis and Characterization of a Double Oximato Bridged Dimeric Copper(II) Complex and Its Use in Oxidative Dimerisation of O-Aminophenol, *Polyhedron*, 2020, **175**, 114164, DOI: **10.1016/j.poly.2019.114164**.

40 S. Roy, M. G. B. Drew, A. Bauzá, A. Frontera and S. Chattopadhyay, Non-Covalent Tetrel Bonding Interactions in Hemidirectional Lead(Ii) Complexes with Nickel(Ii)-Salen Type Metalloligands, *New J. Chem.*, 2018, **42**, 6062–6076, DOI: **10.1039/C7NJ05148D**.

41 S. Roy, M. G. B. Drew, A. Bauzá, A. Frontera and S. Chattopadhyay, Formation of a Water-Mediated Assembly of Two Neutral Copper(Ii) Schiff Base Fragments with a

$Cu_2(NCS)_4$ Moiety: Exploration of Non-Covalent C–H···Π(Bimetallo Ring) Interactions, *CrystEngComm*, 2018, **20**, 1679–1689, DOI: **10.1039/C7CE01473B**.

42 N. Sarkar, M. G. B. Drew, K. Harms, A. Bauzá, A. Frontera and S. Chattopadhyay, Methylene Spacer Regulated Variation in Conformation of Tetradentate N_2O_2 Donor Schiff Bases Trapped in Manganese(Iii) Complexes, *CrystEngComm*, 2018, **20**, 1077–1086, DOI: **10.1039/C7CE02019H**.

43 K. Ghosh, K. Harms, A. Bauzá, A. Frontera and S. Chattopadhyay, Heteronuclear Cobalt(Iii)/Sodium Complexes with Salen Type Compartmental Schiff Base Ligands: Methylene Spacer Regulated Variation in Nuclearity, *Dalton Trans.*, 2018, **47**, 331–347, DOI: **10.1039/C7DT03929H**.

44 S. Thakur, N. Sarkar, M. G. B. Drew, A. Bauzá, A. Frontera and S. Chattopadhyay, Estimating the Energy of Noncovalent Interactions in a Dioxovanadium(V) Schiff Base Complex: Exploration of Its Phenoxazinone Synthase Like Activity, *Polyhedron*, 2018, **142**, 83–92, DOI: **10.1016/j.poly.2017.11.053**.

45 A. Banerjee and S. Chattopadhyay, Dinuclear Mixed Valence Cobalt(II/III) And Hetero-Tetranuclear Cobalt(III)/Na Complexes with A Compartmental Ligand: Synthesis, Characterization and Use as Catalysts for Oxidative Dimerisation of 2-Aminophenol, *Inorg. Chim. Acta*, 2021, **515**, 120044, DOI: **10.1016/j.ica.2020.120044**.

46 K. Ghosh and S. Chattopadhyay, Synthetic Stratagem and Structures of Two Heteroleptic Cobalt(III) Complexes Acting as Biomimetic Catalysts: Role of Co-Ligands in Catalytic Activities, *Polyhedron*, 2019, **170**, 495–507, DOI: **10.1016/j.poly.2019.05.062**.

47 K. Ghosh, K. Harms, A. Franconetti, A. Frontera and S. Chattopadhyay, A Triple Alkoxo Bridged Dinuclear Cobalt(III) Complex Mimicking Phosphatase and Showing Ability to Degrade Organic Dye Contaminants by Photocatalysis, *J. Organomet. Chem.*, 2019, **883**, 52–64, DOI: **10.1016/j.jorganchem.2019.01.006**.

48 T. Basak, A. Bhattacharyya, K. Harms and S. Chattopadhyay, The Ability of a Trinuclear Zinc(II) Schiff Base Complex to Act as A Photocatalyst for The Degradation of Methylene Blue and to Mimic Phosphatase, *Polyhedron*, 2019, **157**, 449–457, DOI: **10.1016/j.poly.2018.09.070**.

49 M. Yuan, F. Zhao, W. Zhang, Z.-M. Wang and S. Gao, Azide-Bridged One-Dimensional Mn^{III} Polymers: Effects of Side Group of Schiff Base Ligands on Structure and Magnetism, *Inorg. Chem.*, 2007, **46**, 11235–11242, DOI: **10.1021/ic701655w**.

50 H. Miyasaka, N. Matsumoto, H. Ōkawa, N. Re, E. Gallo and C. Floriani, Complexes Derived from the Reaction of Manganese(III) Schiff Base Complexes and Hexacyanoferrate(III): Syntheses, Multidimensional Network Structures, and Magnetic Properties, *J. Am. Chem. Soc.*, 1996, **118**, 981–994, DOI: **10.1021/ja952706c**.

51 J. Rakhtshah, A Comprehensive Review on the Synthesis, Characterization, and Catalytic Application of Transition-Metal Schiff-Base Complexes Immobilized on Magnetic Fe_3O_4 Nanoparticles, *Coord. Chem. Rev.*, 2022, **467**, 214614, DOI: **10.1016/j.ccr.2022.214614**.

52 D. Zhang, H. Wang, Y. Chen, Z.-H. Ni, L. Tian and J. Jiang, Hydrogen-Bond Directed Cyanide-Bridged Molecular Magnets Derived from Polycyanidemetalates and Schiff Base Manganese(III) Compounds: Synthesis, Structures, and Magnetic Properties, *Inorg. Chem.*, 2009, **48**, 11215–11225, DOI: **10.1021/ic901530p**.

53 Z. Puterová-Tokárová, V. Mrázová and R. Boča, Magnetism of Novel Schiff-Base Copper(II) Complexes Derived from Aminoacids, *Polyhedron*, 2013, **61**, 87–93, DOI: **10.1016/j.poly.2013.05.045**.

54 D. Karati, S. Mukherjee and S. Roy, An Explicative Review on the Current Advancement in Schiff Base-Metal Complexes as Anticancer Agents Evolved in the Past Decade: Medicinal Chemistry Aspects, *Med. Chem.*, 2023, **19**, 960–985, DOI: **10.2174/1573406419666230707105221**.

55 B. Halder, P. Middya, R. M. Gomila, A. Frontera and S. Chattopadhyay, Synthesis, Structural Characterization, and Theoretical Analysis of Nonconventional Bonding in Dinuclear Zinc(II) Complexes with Tridentate Schiff Bases, *ACS Omega*, 2024, **9**, 41787–41796, DOI: **10.1021/acsomega.4c06136**.

56 M. Gishan, P. Middya, M. G. B. Drew, A. Frontera and S. Chattopadhyay, Synthesis, structural characterization, and theoretical analysis of novel zinc(II) schiff base complexes with halogen and hydrogen bonding interactions, *RSC Adv.*, 2024, **14**, 30896–30911, DOI: **10.1039/D4RA06217E**.

57 P. Middya, A. Frontera and S. Chattopadhyay, The Crucial Role of Hydrogen Bonding in Shaping the Structures of Zinc-Based Coordination Polymers Using Tridentate N, N, O Donor Reduced Schiff Base Ligands and Bridging Acetates, *RSC Adv.*, 2024, **14**, 13905–13914, DOI: **10.1039/D4RA00550C**.

58 P. Middya, M. Karmakar, A. Frontera and S. Chattopadhyay, Insight into The Role of Pseudo-Halides as Multiple Hydrogen Bond Acceptors in The Formation of Supramolecular 1D Assembly of Di and Trinuclear Zinc Complexes, *Inorg. Chim. Acta*, 2023, **553**, 121516, DOI: **10.1016/j.ica.2023.121516**.

59 T. Basak, A. Bhattacharyya, M. Das, K. Harms, A. Bauzá, A. Frontera and S. Chattopadhyay, Phosphatase Mimicking Activity of Two Zinc(II) Schiff Base Complexes with Zn_2O_2 Cores: NBO Analysis and MEP Calculation to Estimate Non-Covalent Interactions, *ChemistrySelect*, 2017, **2**, 6286–6295, DOI: **10.1002/slct.201701246**.

60 H. S. Jena, Diastereoselective Self-Assembly of Heterochiral Zn(Ii) Complexes of Racemic Schiff Bases in a Chiral Self-Discriminating Process: Effect of Non-Covalent Interactions on Solid State Structural Self-Assembly, *RSC Adv.*, 2014, **4**, 3028–3044, DOI: **10.1039/C3RA45082A**.

61 I. Mondal, A. Frontera and S. Chattopadhyay, On the Importance of $RH_3C\cdots N$ Tetrel Bonding Interactions in The Solid State of a Dinuclear Zinc Complex with a Tetradentate Schiff Base Ligand, *CrystEngComm*, 2021, **23**, 3391–3397, DOI: **10.1039/D0CE01864C**.

62 M. Karmakar, A. Frontera and S. Chattopadhyay, Methylene Spacer Regulated Variation in Supramolecular Assembly of Zinc(Ii) Dicyanamide Complexes with Reduced Schiff Base Ligands: Synthesis, Structure and DFT Study, *CrystEngComm*, 2020, **22**, 6876–6885, DOI: **10.1039/D0CE01105C**.

63 M. Azam, S. I. Al-Resayes, A. Trzesowska-Kruszynska, R. Kruszynski, F. Shakeel, S. M. Soliman, M. Alam, M. R. Khan and S. M. Wabaidur, Zn(II) Complex Derived from Bidentate Schiff Base Ligand: Synthesis, Characterization, DFT Studies and Evaluation of Anti-Inflammatory Activity, *J. Mol. Struct.*, 2020, **1201**, 127177, DOI: **10.1016/j.molstruc.2019.127177**.

64 P. Chakraborty, S. Purkait, S. Mondal, A. Bauzá, A. Frontera, C. Masserac and D. Das, Exploration of CH···Π Interactions Involving The Π-System of Pseudohalide Coligands in Metal Complexes of a Schiff-Base Ligand, *CrystEngComm*, 2015, **17**, 4680–4690, DOI: **10.1039/C5CE00795J**.

65 R. S. Sarkar, S. Banerjee and S. Chattopadhyay, Importance of Π-Π Interactions in The Solid State Structures of Two Cobalt Complexes Derived from N,O Donor Reduced Schiff Base Ligands, *Polyhedron*, 2024, **254**, 116916, DOI: **10.1016/j.poly.2024.116916**.

66 M. Karmakar, W. Sk, R. M. Gomila, M. G. B. Drew, A. Frontera and S. Chattopadhyay, An Insight into The Hydrogen Bonding, Halogen Bonding and Chalcogen Bonding Interactions in Manganese(III) Complexes with N_2O_2 Donor Salicylidine Schiff Base Ligands, *RSC Adv.*, 2023, **13**, 21211–21224, DOI: **10.1039/D3RA04044E**.

67 P. Sarmaa, P. Sharmaa, R. M. Gomila, A. Frontera, M. Barcelo-Oliver, A. K. Vermac, B. Baruwa and M. K. Bhattacharyya, Charge Assisted Hydrogen Bonded Assemblies and Unconventional O···O Dichalcogen Bonding Interactions in Pyrazole-Based Isostructural Ni(II) and Mn(II) Compounds Involving Anthraquinone Disulfonate: Antiproliferative Evaluation and Theoretical Studies, *J. Mol. Struct.*, 2022, **1250**, 131883, DOI: **10.1016/j.molstruc.2021.131883**.

68 S. Mirdya, S. Roy, S. Chaterjee, A. Bauzá, A. Frontera and S. Chattopadhyay, Importance of π-Interactions Involving Chelate Rings in Addition to the Tetrel Bonds in Crystal Engineering: A Combined Experimental and Theoretical Study on a Series of Hemi- and Holodirected Nickel(II)/Lead(II) Complexes, *Cryst. Growth Des.*, 2019, **19**, 5869–5881, DOI: **10.1021/acs.cgd.9b00881**.

69 S. Hazra, D. Majumdar, A. Frontera, S. Roy, B. Gassoumi, H. Ghalla and S. Dalai, On the Significant Importance of Hg···Cl Spodium Bonding/σ/π-Hole/Noncovalent Interactions and Nanoelectronic/Conductivity Applications in Mercury Complexes: Insights from DFT Spectrum, *Cryst. Growth Des.*, 2024, **24**, 7246–7261, DOI: **10.1021/acs.cgd.4c00893**.

70 D. Majumdar, A. Frontera, S. Roy and D. Sutradhar, Experimental and Theoretical Survey of Intramolecular Spodium Bonds/σ/π-Holes and Noncovalent Interactions in Trinuclear Zn(II)-Salen Type Complex with OCN– Ions: A Holistic View in Crystal Engineering, *ACS Omega*, 2024, **9**, 1786–1797, DOI: **10.1021/acsomega.3c08422**.

71 S. Roy, A. Bauzá, A. Frontera and S. Chattopadhyay, A Combined Experimental and Computational Study of Supramolecular Assemblies in Two Photoluminescent Cadmium(II) Complexes with Halosalicylaldimine Schiff Bases, *Inorg. Chim. Acta*, 2016, **450**, 321–329, DOI: **10.1016/j.ica.2016.05.030**.

72 Q. Wua, M. Huanga, T. Li, L. Jiaoa, Y. Tua, X. Xua, X. Maa, H. Tiana and Y. Qiao, Crystal and Electronic Structure of Poly-Halogenated Lanthanide Schiff Base Complex: Insights into Halogen Bond from Structural and Theoretical Analysis, *J. Mol. Struct.*, 2021, **1225**, 129054, DOI: **10.1016/j.molstruc.2020.129054**.

73 C. Freire, M. Nunes, C. Pereira, D. M. Fernandes, A. F. Peixoto and M. Rocha, Metallo(Salen) Complexes as Versatile Building Blocks for The Fabrication of Molecular Materials and Devices with Tuned Properties, *Coord. Chem. Rev.*, 2019, **394**, 104–134, DOI: **10.1016/j.ccr.2019.05.014**.

74 W. Wang, Y.-X. Wang and H.-B. Yang, Supramolecular Transformations within Discrete Coordination-Driven Supramolecular Architectures, *Chem. Soc. Rev.*, 2016, **45**, 2656–2693, DOI: **10.1039/C5CS00301F**.

75 H. T. Chifotided and K. R. Dunbar, Anion–π Interactions in Supramolecular Architectures, *Acc. Chem. Res.*, 2013, **46**, 894–906, DOI: **10.1021/ar300251k**.

76 Z. He, W. Jiang and C. A. Schalley, Integrative Self-Sorting: A Versatile Strategy for The Construction of Complex Supramolecular Architecture, *Chem. Soc. Rev.*, 2015, **44**, 779–789, DOI: **10.1039/C4CS00305E**.

77 X.-L. Ni, X. Xiao, H. Cong, Q.-J. Zhu, S.-F. Xue and Z. Tao, Self-Assemblies Based on the "Outer-Surface Interactions" of Cucurbit[n]urils: New Opportunities for Supramolecular Architectures and Materials, *Acc. Chem. Res.*, 2014, **47**, 1386–1395, DOI: **10.1021/ar5000133**.

78 A. Bauzá, I. Alkorta, J. Elguero, T. J. Mooibroek and A. Frontera, Spodium Bonds: Noncovalent Interactions Involving Group 12 Elements, *Angew. Chem., Int. Ed.*, 2020, **59**, 17482–17487, DOI: **10.1002/anie.202007814**.

79 R. M. Gomila, A. Bauzá, T. J. Mooibroek and A. Frontera, Spodium Bonding in Five Coordinated Zn(Ii): A New Player in Crystal Engineering?, *CrystEngComm*, 2021, **23**, 3084–3093, DOI: **10.1039/D1CE00221J**.

80 A. Amonov and S. Scheiner, Spodium Bonding to Dicoordinated Group 12 Atoms, *J. Phys. Chem. A*, 2024, **128**, 8751–8761, DOI: **10.1021/acs.jpca.4c05481**.

81 M. Karmakar, A. Frontera, S. Chattopadhyay, T. J. Mooibroek and A. Bauzá, Intramolecular Spodium Bonds in Zn(II) Complexes: Insights from Theory and Experiment, *Int. J. Mol. Sci.*, 2020, **21**, 7091, DOI: **10.3390/ijms21197091**.

82 R. Llull, G. Montalbán, I. Vidal, R. M. Gomila, A. Bauzá and A. Frontera, Theoretical Study of Spodium Bonding in the Active Site of Three Zn-Proteins and Several Model Systems, *Phys. Chem. Chem. Phys.*, 2021, **23**, 16888–16896, DOI: **10.1039/D1CP02150H**.

83 H. S. Biswas, A. K. Sahu, A. Frontera and A. Bauzá, Spodium Bonds in Biological Systems: Expanding the Role of Zn in Protein Structure and Function, *J. Chem. Inf. Model.*, 2021, **61**, 3945–3954, DOI: **10.1021/acs.jcim.1c00594**.

84 P. Kumar, A. Frontera and S. K. Pandey, Coordination Versus Spodium Bonds in Dinuclear Zn(II) and Cd(II) Complexes with a Dithiophosphate Ligand, *New J. Chem.*, 2021, **45**, 19402–19415, DOI: **10.1039/D1NJ03165A**.

85 T. Basak, R. M. Gomila, A. Frontera and S. Chattopadhyay, Differentiating Intramolecular Spodium Bonds from Coordination Bonds in Two Polynuclear Zinc(II) Schiff Base Complexes, *CrystEngComm*, 2021, **23**, 2703–2710, DOI: **10.1039/D1CE00214G**.

86 G. Mahmoudi, A. Masoudiasl, M. G. Babashkina, A. Frontera, T. Doert, J. M. White, E. Zangrando, F. I. Zubkov and D. A. Safin, On The Importance of Π-Hole Spodium Bonding in Tricoordinated Hg(II) Complexes, *Dalton Trans.*, 2020, **49**, 17547–17551, DOI: **10.1039/D0DT03938A**.

87 P. Middya, M. Karmakar, R. M. Gomila, M. G. B. Drew, A. Frontera and S. Chattopadhyay, The Importance of Spodium Bonds, H-Bonds and π-Stacking Interactions in the Solid State Structures of Four Zinc Complexes with Tetradentate Secondary Diamine Ligands, *New J. Chem.*, 2023, **47**, 9346–9363, DOI: **10.1039/D2NJ05490F**.

88 G. M. Sheldrick, Crystal Structure Refinement with SHELXL, *Acta Crystallogr., Sect. C: Struct. Chem.*, 2015, **71**, 3–8, DOI: **10.1107/S2053229614024218**.

89 G. M. Sheldrick, *SADABS, V2014/5*, Software for Empirical Absorption Correction, University of Göttingen, Institute fur Anorganische Chemieder Universitat, Gottingen, Germany, 1999–2003.

90 A. D. Becke, Density-Functional Exchange-Energy Approximation with Correct Asymptotic Behaviour, *Phys. Rev. A: At., Mol., Opt. Phys.*, 1988, **38**, 3098–3100, DOI: **10.1103/PhysRevA.38.3098**.

91 J. P. Perdew, Density-Functional Approximation for the Correlation Energy of the Inhomogeneous Electron Gas, *Phys. Rev. B: Condens. Matter Mater. Phys.*, 1986, **33**, 8822–8824, DOI: **10.1103/PhysRevB.33.8822**.

92 S. Grimme, J. Antony, S. Ehrlich and H. Krieg, A Consistent and Accurate Ab Initio Parametrization of Density Functional Dispersion Correction (DFT-D) For The 94 Elements H-Pu, *J. Chem. Phys.*, 2010, **132**, 154104, DOI: **10.1063/1.3382344**.

93 F. Weigend, Accurate Coulomb-Fitting Basis Sets for H to Rn, *Phys. Chem. Chem. Phys.*, 2006, **8**, 1057–1065, DOI: **10.1039/B515623H**.

94 R. Ahlrichs, M. Bär, M. Häser, H. Horn and C. Kölmel, Electronic Structure Calculations on Workstation Computers: The Program System Turbomole, *Chem. Phys. Lett.*, 1989, **162**, 165–169, DOI: **10.1016/0009-2614(89)85118-8**.

95 R. F. W. Bader, A Quantum Theory of Molecular Structure and its Applications, *Chem. Rev.*, 1991, **91**, 893–928, DOI: **10.1021/cr00005a013**.

96 E. R. Johnson, S. Keinan, P. Mori-Sánchez, J. Contreras-García, A. J. Cohen and W. Yang, Revealing Noncovalent Interactions, *J. Am. Chem. Soc.*, 2010, **132**, 6498–6506, DOI: **10.1021/ja100936w**.

97 T. Lu and F. Chen, Multiwfn: A Multifunctional Wavefunction Analyser, *J. Comput. Chem.*, 2012, **33**, 580–592, DOI: **10.1002/jcc.22885**.

98 W. Humphrey, A. Dalke and K. Schulten, VMD: Visual Molecular Dynamics, *J. Mol. Graphics*, 1996, **14**, 33–38, DOI: **10.1016/0263-7855(96)00018-5**.

99 E. D. Glendening, C. R. Landis and F. Weinhold, NBO 7.0: New Vistas in Localized and Delocalized Chemical Bonding Theory, *J. Comput. Chem.*, 2019, **40**, 2234–2241, DOI: **10.1002/jcc.25873**.

100 E. D. Glendening, J. K. Badenhoop, A. E. Reed, J. E. Carpenter, J. A. Bohmann, C. M. Morales, P. Karafiloglou, C. R. Landis and F. Weinhold, *NBO 7.0.*, Theoretical Chemistry Institute, University of Wisconsin, Madison, 2018.

101 Z.-L. You, H.-L. Zhu and W.-S. Liu, Solvolthermal Syntheses and Crystal Structures of Three Linear Trinuclear Schiff Base Complexes of Zinc(II) and Cadmium(II), *Z. Anorg. Allg. Chem.*, 2004, **630**, 1617, DOI: **10.1002/zaac.200400125**.

102 S. Ponsico, H. Gulyas, M. Martnez-Belmonte, E. C. Escudero-Adan, Z. Freixa and P. W. N. M. van Leeuwen, Zn(II) Robson Macrocycles as Templates for Chelating Diphosphines, *Dalton Trans.*, 2011, **40**, 10686, DOI: **10.1039/C1DT10905G**.

103 S. Majumder, L. Mandal and S. Mohanta, Syntheses, Structures, and Steady State and Time Resolved Photophysical Properties of a Tetraiminodiphenol Macrocyclic Ligand and Its Dinuclear Zinc(II)/Cadmium(II) Complexes with Coordinating and Noncoordinating Anions, *Inorg. Chem.*, 2012, **51**, 8739–8749, DOI: **10.1021/ic300412u**.

104 B. Miroslaw, B. Cristovao and Z. Hnatejko, Heterometallic Zn^{II}–Ln^{III}–Zn^{II} Schiff Base Complexes with Linear or Bent Conformation—Synthesis, Crystal Structures, Luminescent and Magnetic Characterization, *Molecules*, 2018, **23**, 1761, DOI: **10.3390/molecules23071761**.

105 K. Zhang, H. Qian, L. Zhang and W. Huang, Influence of the Pendant Arm, Halide, and Solvent on High-Efficient-Tuning [1 + 1] and [2 + 2] Schiff-Base Macrocyclic Complexes via a Zinc-Ion Template, *Inorg. Chem.*, 2015, **54**, 675–681, DOI: **10.1021/ic502642q**.

106 M. Azam and S. I. Al-Resayes, Phenoxy-Bridged Binuclear Zn(II) Complex Holding Salen Ligand: Synthesis and Structural Characterization, *J. Mol. Struct.*, 2016, **1107**, 77, DOI: **10.1016/j.molstruc.2015.11.017**.

107 D. Majumdar, M. S. S. Babu, S. Das, J. K. Biswas, M. Mondal and S. Hazra, Synthesis, X-Ray Crystal Structure, Photo Luminescent Property, Antimicrobial Activities and DFT Computational Study Of Zn(II) Coordination Polymer Derived from Multisite N,O Donor Schiff Base Ligand (H_2L^1), *J. Mol. Struct.*, 2017, **1138**, 161–171, DOI: **10.1016/j.molstruc.2017.03.017**.

108 G. Consiglio, S. Failla, P. Finocchiaro, I. P. Oliveri, R. Purrello and S. D. Bella, Supramolecular Aggregation/Deaggregation in Amphiphilic Dipolar Schiff-Base Zinc(II) Complexes, *Inorg. Chem.*, 2010, **49**, 5134–5142, DOI: **10.1021/ic100284r**.

109 G. Consiglio, I. P. Oliveri, S. Failla and S. D. Bella, Supramolecular Aggregates of Defined Stereochemical Scaffolds: Aggregation/Deaggregation in Schiff-Base Zinc(II) Complexes Derived from Enantiopure trans-1,2-Diaminocyclohexane, *Inorg. Chem.*, 2016, **55**, 10320–10328, DOI: **10.1021/acs.inorgchem.6b01580**.

110 T. Basak, D. Das, P. P. Ray, S. Banerjee and S. Chattopadhyay, Synthesis, Characterization, Self-Assembly and Non-Ohmic Schottky Barrier Diode Behaviors of two Iron(III) Based Semiconductors with Theoretical Insight, *CrystEngComm*, 2020, **22**, 5170–5181, DOI: **10.1039/D0CE00223B**.

111 M. Karmakar, T. Basak and S. Chattopadhyay, Phosphatase-Mimicking Activity of a Unique penta-Nuclear Zinc(II) Complex with a Reduced Schiff Base Ligand: Assessment of its Ability to Sense Nitroaromatics, *New J. Chem.*, 2019, **43**, 4432–4443, DOI: **10.1039/C8NJ06549G**.

112 A. Banerjee, A. Frontera and S. Chattopadhyay, Methylene Spacer Regulated Variation in Molecular and Crystalline Architectures of Cobalt(Iii) Complexes with Reduced Schiff Base Ligands: A Combined Experimental and Theoretical Study, *Dalton Trans.*, 2019, **48**, 11433–11447, DOI: **10.1039/C9DT01818B**.

113 A. Hazari, L. K. Das, R. M. Kadam, A. Bauzá, A. Frontera and A. Ghosh, Unprecedented Structural Variations in Trinuclear Mixed Valence Co(II/III) Complexes: Theoretical Studies, Pnicogen Bonding Interactions and Catecholase-Like Activities, *Dalton Trans.*, 2015, **44**, 3862–3876, DOI: **10.1039/C4DT03446E**.

114 K. Visvaganesan, R. Mayilmurugan, E. Suresh and M. Palaniandavar, Iron(III) Complexes of Tridentate 3N Ligands as Functional Models for Catechol Dioxygenases: The Role of Ligand N-alkyl Substitution and Solvent on Reaction Rate and Product Selectivity, *Inorg. Chem.*, 2007, **46**, 10294–10306, DOI: **10.1021/ic700822y**.

115 L. Yang, D. R. Powell and R. P. Houser, Structural Variation in Copper(I) Complexes with Pyridylmethylamide Ligands: Structural Analysis with a New Four-Coordinate Geometry Index, τ_4, *Dalton Trans.*, 2007, 955–964, DOI: **10.1039/B617136B**.

116 A. W. Addison, T. N. Rao, J. Reedijk, J. van Rijn and G. C. Verschoor, Synthesis, Structure and Spectroscopic Properties of Copper(II) Compounds Containing Nitrogen–Sulphur Donor Ligands; The Crystal and Molecular Structure of Aqua[1,7-Bis(N-Methylbenzimidazol-2′-Yl)-2,6-Dithiaheptane]Copper(II) Perchlorate, *J. Chem. Soc., Dalton Trans.*, 1984, 1349–1356, DOI: **10.1039/DT9840001349**.

117 D. Cremer and J. A. Pople, General Definition of Ring Puckering Coordinates, *J. Am. Chem. Soc.*, 1975, **97**, 1354–1358, DOI: **10.1021/ja00839a011**.

118 D. Cremer, On The Correct Usage of the Cremer-Pople Puckering Parameters as Quantitative Descriptors of Ring Shapes - a Reply to Recent Criticism by Petit, Dillen and Geise, *Acta Crystallogr., Sect. B: Struct. Sci.*, 1984, **40**, 498–500, DOI: **10.1107/S0108768184002548**.

119 A. Mallick and N. Chattopadhyay, Photophysics in Motionally constrained Bioenvironment: Interactions of Norharmane with Bovine Serum Albumin, *Photochem. Photobiol.*, 2005, **81**, 419–424, DOI: **10.1111/j.1751-1097.2005.tb00202.x**.

120 H. A. Benesi and J. H. Hildebrand, A Spectrophotometric Investigation of the Interaction of Iodine with Aromatic Hydrocarbons, *J. Am. Chem. Soc.*, 1949, **71**, 2703–2707, DOI: **10.1021/ja01176a030**.

121 Z.-J. Wang, L. Qin, J.-X. Chen and H.-G. Zheng, H-Bonding Interactions Induced Two Isostructural Cd(II) Metal–Organic Frameworks Showing Different Selective Detection of Nitroaromatic Explosives, *Inorg. Chem.*, 2016, **55**, 10999–11005, DOI: **10.1021/acs.inorgchem.6b01521**.

122 H. Wang, W. Yang and Z.-M. Sun, Mixed-Ligand Zn-MOFs for Highly Luminescent Sensing of Nitro Compounds, *Chem. – Asian J.*, 2013, **8**, 982–989, DOI: **10.1002/asia.201201184**.

123 D. Ma, B. Li, X. Zhou, Q. Zhou, K. Liu, G. Zeng, G. Li, Z. Shi and S. Feng, A Dual Functional MOF as A Luminescent Sensor for Quantitatively Detecting the Concentration of Nitrobenzene and Temperature, *Chem. Commun.*, 2013, **49**, 8964–8966, DOI: **10.1039/C3CC44546A**.

124 B. Gole, A. K. Bar and P. S. Mukherjee, Fluorescent Metal–Organic Framework for Selective Sensing of Nitroaromatic Explosives, *Chem. Commun.*, 2011, **47**, 12137–12139, DOI: **10.1039/C1CC15594F**.

125 D. Tian, Y. Li, R.-Y. Chen, Z. Chang, G.-Y. Wang and X.-H. Bu, A Luminescent Metal–Organic Framework Demonstrating Ideal Detection Ability for Nitroaromatic Explosives, *J. Mater. Chem. A*, 2014, **2**, 1465–1470, DOI: **10.1039/C3TA13983B**.

126 G.-Y. Wang, C. Song, D.-M. Kong, W.-J. Ruan, Z. Chang and Y. Li, Two Luminescent Metal–Organic Frameworks for the Sensing of Nitroaromatic Explosives and DNA Strands, *J. Mater. Chem. A*, 2014, **2**, 2213–2220, DOI: **10.1039/C3TA14199C**.

127 Y.-C. He, H.-M. Zhang, Y.-Y. Liu, Q.-Y. Zhai, Q.-T. Shen, S.-Y. Song and J.-F. Ma, Luminescent Anionic Metal–Organic Framework with Potential Nitrobenzene Sensing, *Cryst. Growth Des.*, 2014, **14**, 3174–3178, DOI: **10.1021/cg5004353**.